Journal of Applied Polymer Science

WILEY

Applied Polymer SCIENCE

RESEARCH ARTICLE OPEN ACCESS

Argon Cold Plasma Modification of Polyethylene Films to Tailor Surface and Barrier Properties

Aikaterini Spanou[1] | Chrysi Lagkouvardou[1] | Petrina Vogiannou[1] | Vasiliki Korka[1] | Enrico Maurizzi[2,3] | Ioanna Georgia I. Athanasoulia[4] | Dimitrios Ladakis[5] | Andrea Pulvirenti[2,3] | Efstathios Z. Panagou[6] | Demetres Briassoulis[4] | Apostolis Koutinas[1] | Theofania Tsironi[1]

[1]Laboratory of Food Process Engineering, Department of Food Science and Human Nutrition, Agricultural University of Athens, Athens, Greece | [2]Department of Life Sciences, University of Modena and Reggio Emilia, Reggio Emilia, Italy | [3]Interdepartmental Research Centre for the Improvement of Agro-Food Biological Resources (BIOGEST-SITEIA), University of Modena and Reggio Emilia, Reggio Emilia, Italy | [4]Laboratory of Farm Structures, Department of Natural Resources Development and Agricultural Engineering, Agricultural University of Athens, Athens, Greece | [5]Department of Agriculture Development, Agri-Food and Natural Resources Management, National and Kapodistrian University of Athens, Psahna Evias, Greece | [6]Laboratory of Microbiology and Biotechnology of Foods, Department of Food Science and Human Nutrition, Agricultural University of Athens, Athens, Greece

Correspondence: Theofania Tsironi (ftsironi@aua.gr)

Received: 5 October 2025 | **Revised:** 23 January 2026 | **Accepted:** 23 January 2026

Keywords: cold plasma | packaging applications | polyolefins | surfaces and interfaces

ABSTRACT

Polyethylene (PE) films are widely used in packaging but require surface modification to improve interfacial adhesion with coatings or laminates that enhance their inherently limited barrier properties. In this study, low-density (LDPE) and high-density polyethylene (HDPE) films are treated with argon (Ar) cold atmospheric plasma (CAP) using a jet-type device, and their properties are characterized prior to and post processing. While plasma exposure enhances wettability by halving the water contact angle (WCA) and increasing surface free energy (SFE), it compromises the film surface structure, increasing water vapor and oxygen permeability by up to 60% and 45%, respectively. Aging tests reveal partial recovery of hydrophobicity, though WCAs stabilize below the untreated values. FTIR spectra indicate the formation of polar groups (hydroxyl and carbonyl) after 10–30 min of treatment, accompanied by increased crystallinity. SEM shows pronounced surface etching and morphological alterations, consistent with roughness analysis, which displays a sharp rise after 10 min followed by a slight decrease at 30 min. Antimicrobial capacity remains limited, while long-term degradation results in minimal weight loss (WL), despite sustaining low WCAs. Overall, although CAP treatment impairs the film intrinsic structure, it significantly improves surface chemistry and topography for interfacial bonding, thus optimizing multilayer packaging applications.

1 | Introduction

Polymeric materials play a crucial role in the food industry and they are especially preferred for food packaging applications due to their desirable properties, such as flexibility, transparency, gas and moisture barriers, and chemical inertness, with polyethylene terephthalate (PET), polyethylene (PE), polypropylene (PP), polyvinyl chloride (PVC), and polystyrene (PS) being the most commonly used [1, 2]. However, the latter advantage inevitably leads to very low surface energy and, consequently, poor adhesive properties, particularly in the case of polyolefins, thus requiring surface treatments to improve their wettability [3, 4]. Cold plasma (CP) treatment can modify polymer surfaces by altering their topography and chemistry, effectively forming a functionalized "new layer" at the nanometer scale, resulting in materials with enhanced adhesiveness and desired packaging features, while also providing surface sterilization [5, 6]. However, the characterization of surface modifications induced by CP treatment, particularly in relation to

bulk and mass transport properties that determine the effectiveness as food packaging materials, remains an understudied area. Therefore, further research is crucial not only for designing novel packaging solutions for different food types but also for optimizing the pretreatment steps required to bond barrier-enhancing coatings or laminates onto inert polyolefin films [7–11].

The surface modification mechanism of polymers by CP treatment primarily involves interactions between radicals and ions, and the polymer surface [12, 13]. These interactions alter the surface's chemical and physical properties through functionalization via the addition of active species, as well as processes such as surface ablation, etching, cross-scission, crosslinking and degradation [4, 5, 14]. A type of plasma functionalization is plasma activation, a generic term that refers to plasma treatments that can increase the surface free energy (SFE) via the addition or substitution of surface elements, such as atoms and molecules. Generally, in reactive plasmas, two types of active species exist: (1) reactive ions and radicals, which directly incorporate new functional groups onto surfaces, and (2) nonreactive species (e.g., photons, electrons) that do not directly modify surfaces. Plasmas generated from reactive gases (e.g., O_2, N_2) contain both reactive and nonreactive species, whereas plasmas from inert gases (e.g., Ar, He) include only nonreactive species. However, these nonreactive species can generate radicals on the surface by reacting with ambient oxygen or water, leading to the incorporation of functional groups onto the polymer's surface [15]. Additionally, surface roughness induced by the plasma treatment can affect the surface wettability, thus improving its adhesive performance [4, 16]. Surface etching caused by plasma involves the removal of material and the formation of gas-phase products through bombardment of the surface by high-energy ions, neutrals, and electron impacts, while it is classified into chemical etching, where plasma-activated gases react with the surface, and physical etching, where accelerated plasma ions collide onto the surface [15, 17]. The latter mechanism is particularly notable in the case of Ar plasma [18]. Nevertheless, in the specific case of PE, studies have shown that the extent of mass loss remains lower compared to oxygen-containing polymers under equivalent plasma exposure [19].

Polyolefins, due to their broad applicability, low surface energy, and complete lack of functional groups, represent the most extensively studied polymer class in plasma surface treatment research [20]. When PE is exposed to CP, the mechanisms of surface modification depend strongly on generic parameters such as energy density, pressure and discharge gas, but also on the polymer substrate [17]. The latter has been demonstrated by Švorčík et al. who found that the chemical structure of PE can further influence the extent of modification, since low-density (LDPE) and high-density polyethylene (HDPE) exhibit distinct wettability, cross-linking degrees, oxygen incorporation levels, and surface roughness under identical Ar plasma conditions [13]. Inert gases such as Ar theoretically do not directly incorporate functional groups onto the polymer surface, in contrast to reactive gases like oxygen or nitrogen [17]. Instead, their primary chemical action is hydrogen abstraction (a characteristic reaction in aliphatic chains [21]), which generates surface radicals without interacting with them, thereby favoring cross-linking and the formation of conjugated double bonds [20–22]. While these radicals may subsequently react with atmospheric oxygen to yield peroxide, carboxyl, hydroxyl, and carbonyl functionalities, the degree of such oxygen-containing group incorporation remains lower than that obtained with reactive gas plasmas [17, 22]. According to Yao et al. the rate of cross-linking in HDPE has been reported to follow the trend $Ar > H_2 > O_2 > N_2 = air$, highlighting the efficiency of Ar in promoting this process [23]. For PE, the dominant plasma-induced reaction pathway favors the formation of cross-links within the polymer matrix, as opposed to significant double-bond formation, which is more characteristic of other polymer classes [24]. Generally, in polyolefins, regardless of the gas used for the plasma treatment, radical generation occurs either through C–C or C–H bond dissociation; the former pathway leads to functionalization accompanied by degradation, whereas the latter results in functionalization alone, which could further lead to cross-linking [17, 20, 25]. Given the similar bond dissociation energies of C–C and C–H bonds, precise control of plasma parameters is essential to achieve the desired surface modification without excessive degradation [17]. These interrelated chemical processes (cross-linking, double-bond formation, limited oxidative functionalization, and etching) collectively determine the surface chemistry of PE following Ar CP activation.

Besides the immediate effects of plasma treatment on polymer surfaces, longer-term phenomena such as structural changes and hydrophobic recovery (HR) occur [21]. HR, also known as aging, describes the gradual reversal of the increased surface polarity and wettability, as the surface tends to return partially or fully to its original hydrophobic state due to physical aging processes [21]. This spontaneous process that occurs after the plasma treatment is thermodynamically driven and attributed to factors such as surface reactions causing structural modifications and chain rearrangements, exposure to UV irradiation, and the presence of highly oxidative gaseous species [16, 26].

The aim of the present study is to evaluate the effect of Ar atmospheric pressure CP on the surface and mass transport properties of commercially available LDPE and HDPE, two widely used types of polyethylene in food packaging. An atmospheric pressure plasma jet (APPJ) was employed for the treatment, a configuration that has become increasingly popular due to its low cost, ease of integration into production lines, and ability to provide uniform treatment not only for flat, thin 2D surfaces but also for complex structures [5, 27–29]. The properties studied for surface characterization of the materials included static WCA and SFE to assess wettability, as well as surface morphology, chemical composition, and the aging effect under different conditions–properties that have been previously investigated in the literature, while also, mass transport properties, such as water vapor and oxygen permeabilities, were measured to address the existing gap in the literature.

2 | Methods

2.1 | Experimental Details

2.1.1 | Materials

Commercially available low-density polyethylene (LDPE, 40 μm thick) and high-density polyethylene (HDPE, 20 μm thick) films were used for this experiment.

2.1.2 | Cold Atmospheric Plasma (CAP) Processing

The films were treated with Ar CAP using a kINPen IND jet device (neoplas control GmbH, Greifswald, Germany), equipped with a conical metal nozzle (Ø 16 cm, height 6 cm) to ensure uniform treatment (Figure 1). The device features a central RF-powered electrode (13.56 MHz) enclosed in a dielectric ceramic tube and a grounded outer cylindrical electrode. Plasma is generated between the pointed 1 mm central electrode and the nozzle outlet (~3.5 mm distance). The capillary has an internal diameter of 1.6 mm and protrudes ~2 mm beyond the nozzle head. The unit operates with noble gases (Ar or He), at a gas flow rate between 3 and 5 L/min and typical plasma power between 0.3 and 3.5 W, with visible plasma length of 9–13 mm in pure Ar. The entire system power is ~20 W [30].

The film samples were cut to dimensions of 2 × 8 cm and positioned beneath the plasma jet nozzle for treatment. The plasma operated at a temperature of approximately 35°C, using high-purity Ar gas (Argon 4.8; 99.998%; Buse Gas SA, Schimatari, Greece) as the feed gas. A fixed distance of 10 mm was maintained between the plasma source and the sample surface. The conical nozzle attached to the jet ensured uniform treatment and enhanced process repeatability. The Ar flow rate was set at 4 L/min. Two treatments (10 and 30 min) were applied on one side of each membrane.

2.2 | Surface Chemistry Characterization

Fourier transform infrared spectroscopy with attenuated total reflectance mode (FTIR-ATR) was used to qualitatively investigate surface chemical modifications on plasma-treated LDPE and HDPE films. A VERTEX 70 FTIR spectrometer (Bruker Optik GmbH, Ettlingen, Germany) equipped with an ATR probe was used for this analysis. Spectra were recorded in the range of 4000–600 cm^{-1} with a spectral resolution of 2 cm^{-1} by averaging 64 scans per measurement. Only the treated side of each film was examined, and all measurements were performed in triplicate. Post-acquisition processing was conducted using SpectraGryph v1.2.16.1. Spectra were averaged (by mean), baseline-corrected automatically with a single-run adaptive algorithm (coarseness = 9, offset = −1), smoothed using the Savitzky–Golay algorithm (2nd order, 9-point window), and normalized by area.

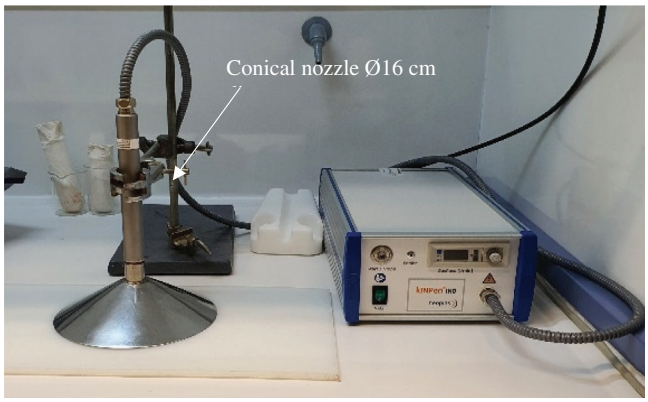

FIGURE 1 | Configuration of the kINPen IND system with the attached conical nozzle. [Color figure can be viewed at wileyonlinelibrary.com]

2.3 | Degree of Crystallinity Estimation

The degree of crystallinity of LDPE and HDPE films was estimated using the empirical method proposed by Zerbi et al. based on analysis of the characteristic infrared absorption band doublets at 1472/1462 and 729/719 cm^{-1} [31]. In this method, the 1472 and 729 cm^{-1} bands are attributed to the crystalline phase, while the 1462 and 719 cm^{-1} bands correspond to the amorphous phase. The crystallinity index was calculated using intensity ratios of the respective peaks, assuming a value of 1.233 for the band ratio in fully crystalline polyethylene. The following empirical expression was used for the calculation:

$$X = \frac{1 - \frac{\frac{I_a}{I_b}}{1.233}}{1 + \frac{I_a}{I_b}} \times 100 \quad (1)$$

where X is the percentage of the amorphous phase, and I_α/I_b are the infrared intensities in the spectral bands of doublets 1472/1462 or 729/719 cm^{-1}.

The peak components were deconvoluted assuming a weighted mixture of the Lorentzian–Gaussian functions, and the fitting parameters (relative weight, height, width, and position of each peak) were optimized using a nonlinear least-squares algorithm to ensure optimal fitting between the summed spectral profile and the experimental spectrum [32, 33]. The peak deconvolution in both regions was optimized by selecting the solution that provided the best overall agreement with the experimental spectrum ($R^2 > 0.99$), while the extracted peak parameters remained within ranges consistent with previous reports, ensuring that the calculated crystallinity values are directly comparable to those in the literature [32, 34]. No full peak decomposition of the two regions was performed. Although this approach would in principle separate orthorhombic, amorphous, and monoclinic-like contributions, it is highly dependent on external reference spectra (e.g., crystalline orthorhombic n-alkanes) or on complementary thermal characterization to constrain the hidden, strongly overlapping bands, and without such references, the fitting remains largely assumption-driven [31, 34–36]. Moreover, the deconvolution of the 1472/1462 cm^{-1} doublet included a third peak at 1442 cm^{-1}, which is attributed to gauche conformers present in the polymer, reflecting regions of the amorphous phase [31]. The peak deconvolution was performed using custom Python scripts (v3.11) executed in the IDLE environment (Python Software Foundation, https://www.python.org/).

2.4 | Surface Morphology Analysis

Scanning electron microscopy (SEM) was employed to obtain high-resolution 2D images of the sample surfaces. A Nova NanoSEM 450 microscope (FEI, Hillsboro, OR, USA) was used for the analyses. Prior to imaging, a thin gold (Au) coating (10 nm) was sputter-deposited on the LDPE and HDPE film samples to prevent charging and enhance image quality. Samples

were mounted on stainless steel stubs using double-sided conductive carbon tape. Imaging was performed under high vacuum conditions (HiVac mode, 10^{-2}–10^{-4} Pa) at an accelerating voltage of 8 kV and at magnifications of 40,000× and 100,000×.

For the assessment of surface roughness, the SurfCharJ 1q plugin (available at https://www.gcsca.net/IJ/SurfCharJ.html), developed by Chinga et al. for the ImageJ software, was used [37, 38]. SEM micrographs were first converted to 32-bit format and properly scaled prior to analysis [39]. The plugin was then used to calculate root mean square roughness (R_q), arithmetic mean roughness or arithmetic average height (R_a), maximum valley depth (R_v), maximum peak height (R_p), and maximum height of the profile (R_{max}) [40]. The analysis was performed with options for surface leveling, local roughness evaluation (sampling lengths of 350 and 500 nm were applied for LDPE and HDPE, respectively, according to the characteristic size of the surface features), and gradient analysis, while no additional filters were applied [41]. Roughness parameters were determined over the entire micrographs acquired at 40,000× magnification, in order to capture representative topographical variations and to avoid bias from local heterogeneities. In addition, the 3D Interactive Surface Plot plugin in ImageJ (available at https://imagej.net/ij/plugins/surface-plot-3d.html) was utilized to produce representative three-dimensional reconstructions of the film surfaces.

2.5 | Surface Wettability Measurements

2.5.1 | Hydrophilicity

The surface hydrophobicity of the films was evaluated by measuring the static *WCA* using a Theta Flow Optical Tensiometer (Biolin Scientific AB, Gothenburg, Sweden). A 4 μL drop of deionized water (diH_2O) was deposited onto the plasma-treated side of each film using the sessile drop method. Films were affixed onto standard microscope glass slides (75 × 26 mm) with double-sided adhesive tape and placed on the sample stage of the instrument.

A high-resolution camera recorded the drop profile for 10 s at a frame rate of 6 FPS. The contact angle was calculated using the OneAttension software as the mean value from all recorded frames. The static angle was measured based on Young's equation, which assumes that interfacial forces are thermodynamically stable. For each treatment, WCA was determined from 20 drops distributed across three replicate film samples.

All measurements were conducted under ambient conditions (23.7°C ± 0.3°C, *RH* 52.3% ± 1.7%).

2.5.2 | Surface Free Energy (SFE)

To further evaluate the surface properties of the plasma-treated films, the total *SFE* and its polar and dispersive components were calculated using the Owens–Wendt–Rabel–Kaelble (OWRK) model [42, 43]. For this purpose, static contact angle measurements were conducted using test liquids with different surface tensions, namely diiodomethane and ethylene glycol, in addition to water (their known surface energy parameters are given in Table 1). The measurements were performed in the same manner as described for *WCA* determination.

The OWRK method is based on the geometric mean approach, whereby the total SFE γ is expressed as the sum of its dispersive γ^d and polar γ^d components for both surface tensions of the solid and the liquid materials (γ_s and γ_l, respectively) as described by the equations below:

$$\gamma_s = \gamma_s^d + \gamma_s^p \tag{2}$$

$$\gamma_l = \gamma_l^d + \gamma_l^p \tag{3}$$

According to the Young and Owens–Wendt equations, the relationship between the liquid–solid contact angle (θ) and the surface tension components is:

$$\left(\gamma_l^d + \gamma_l^p\right)(1 + \cos\theta) = 2\sqrt{\gamma_s^d\,\gamma_l^d} + 2\sqrt{\gamma_s^p\,\gamma_l^p} \tag{4}$$

By rearranging the above expression into linear form, the SFE components of the solid were determined through linear regression analysis using the measured contact angles and the known surface tension parameters of the probe liquids. Specifically, the equation was transformed into the form $y = mx + c$ (by subsequent substitution in the Young's equation $\gamma_s = \gamma_s^l + \gamma_l \cos\theta$) allowing the polar and dispersive components to be extracted from the slope and intercept of the fitted line (See Equation 5). The use of three liquids with varying polar/dispersive ratios enhances the linearity and accuracy of the model while minimizing errors related to fluid selection [5, 45–47].

$$\frac{(1 + \cos\theta)\gamma_l}{2\sqrt{\gamma_l^d}} = \sqrt{\gamma_s^p}\sqrt{\frac{\gamma_l^p}{\gamma_l^d}} + \sqrt{\gamma_s^d} \tag{5}$$

2.5.3 | Aging

Plasma-treated polymeric surfaces are known to undergo temporal changes due to surface energy relaxation, a phenomenon commonly referred to as aging [26, 48]. This process is characterized by a gradual reduction of SFE, leading to a partial recovery of the original hydrophobicity. The primary mechanisms driving aging include polymer chain reorientation, migration of polar functional groups, and exposure to environmental factors such as temperature and humidity [48, 49].

TABLE 1 | Surface tension components of the testing liquids at 20°C [44].

Liquids	γ_l (mJ m^{-2})	γ_l^p (mJ m^{-2})	γ_l^s (mJ m^{-2})
Water (W)	72.8	51.0	21.8
Diiodomethane (DM)	50.8	0	50.8
Ethylene glycol (EG)	48.0	29.0	19.0

In this study, aging was monitored by WCA measurements on samples treated with Ar plasma for 30 min -identified as the most effective condition yielding the lowest initial *WCA* values. To simulate realistic storage scenarios, samples were stored under different combinations of temperature and relative humidity (RH), using sealed glass desiccators containing saturated salt solutions of $Mg(NO_3)_2{\cdot}6H_2O$ and $BaCl_2{\cdot}2H_2O$. Two temperature conditions were applied: ambient (25°C) and refrigerated (5.0°C). The corresponding *RH* levels were derived from established equilibrium data and are summarized in Table 2 [50–53].

Samples were mounted on microscope glass slides and, immediately after the CAP treatment, were stored in their respective environments for 18 days. WCA was measured at regular intervals (3 days) to monitor the evolution of surface wettability over time, enabling the assessment of wettability recovery as a function of storage duration.

2.6 | Barrier Properties

2.6.1 | Water Vapor Permeability (WVP)

The water vapor transmission rate (WVTR) of the films was determined gravimetrically using the desiccant method, following the ASTM E96/E96M-14 standard with slight modifications [54]. Polyethylene films were sealed over the openings of 25 mL glass vials containing approximately 2.5 g of anhydrous calcium chloride ($CaCl_2$). The vials were placed inside airtight glass containers with saturated aqueous $BaCl_2$ solution, maintaining a RH of ~90% at 25°C [51, 52]. The entire system was stored in a temperature-controlled chamber, and WVTR was estimated at two different temperatures: 25°C ± 1°C and 30°C ± 1°C. The increase in the mass of each vial was recorded at regular intervals (24 h) over a period of 40 days using an analytical balance with 0.0001 g precision. For each sample type, seven replicate vials were prepared and analyzed to ensure statistical reliability of the measurements.

The WVTR was calculated from the slope of the linear portion of the weight gain vs. time curve, normalized to the exposed surface area of the film, and expressed in g m^{-2} day^{-1}, using the Equation (6):

$$\mathrm{WVTR} = \frac{G}{t \times A} \tag{6}$$

where G is the mass gain (g), t the time (days), and A the film area (m^2).

TABLE 2 | Relative humidity of saturated salt solutions [50–53].

Saturated salt solution (aq.)	Temperature (°C)	Relative humidity (%RH)
$BaCl_2{\cdot}2H_2O$	25.0	90.0–90.3
$BaCl_2{\cdot}2H_2O$	5.0	93.0
$Mg(NO_3)_2{\cdot}6H_2O$	25.0	52.9–53.4
$Mg(NO_3)_2{\cdot}6H_2O$	5.0	58.9–59.2

WVP was then calculated as:

$$\mathrm{WVP} = \frac{\mathrm{WVTR} \times L}{\Delta p} = \frac{\mathrm{WVTR} \times L}{S\left(R_1 - R_2\right)} \tag{7}$$

where L is the film thickness (m), Δp the water vapor pressure difference across the film (kPa) (was calculated as 2.85165 kPa for 25°C and 3.8205 kPa for 30°C), S the saturation vapor pressure at test temperature (kPa), R_1 and R_2 the RH at the source and the vapor sink, respectively. The units of WVP are expressed as g mm m^{-2} day^{-1} kPa^{-1}.

2.6.2 | Oxygen Transmission Rate (OTR)

Oxygen Transmission Rate (OTR) was determined using a static accumulation method adapted from ASTM E2945-14, with slight modifications, and analyzed by gas chromatography (GC) [55]. A Shimadzu 2010 (Shimadzu Corporation, Kyoto, Japan) equipped with a thermal conductivity detector (TCD) and a Carboxen 1010 PLOT fused silica capillary column (30 m × 0.32 mm) was used for the quantification of oxygen in all analyses. Data acquisition and processing were performed using GC Solution software. For each analysis, 100 µL of the headspace gas sample was injected in split mode at 120°C into the GC injector. Helium was used as the carrier gas at a flow rate of 8 mL/min.

The test apparatus, primarily based on the designs of Papiernik et al. with additional features from Zeman and Kubik, consisted of a cylindrical stainless steel diffusion cell with an internal diameter of 150 mm and a total volume of 4 L. [56–58] The cell was divided into two equal compartments (2 L each), a source chamber and a collection chamber, by clamping the test film between the two halves. The two halves were joined together at a flange, where bolts and nuts tightened the assembly with silicone diaphragms acting as gaskets to ensure airtight sealing of the chambers. Each compartment had one inlet and one outlet port, with one of the ports also functioning as a sampling port sealed with a septum. Prior to testing, one compartment was filled with high-purity oxygen and the other with high-purity nitrogen by flowing the respective gases through the inlet for approximately 1 min while the outlet was open, ensuring the complete replacement of the chamber atmosphere. Afterwards, the gas flow was stopped, the outlet was simultaneously closed, and then the inlet was carefully sealed to prevent any air ingress during the test. RH inside the chamber was maintained at 0% using silica gel pellets, while all the analyses were carried out at 23°C ± 0.5°C.

Oxygen permeation was monitored over time by periodically sampling the collection chamber headspace (N_2 side) and analyzing the oxygen content by GC. For LDPE films, measurements were taken every 24 h for a total of 7 days, while for HDPE films, measurements were taken every 24 h for a total of 3 days, reflecting the higher transmission rate observed for HDPE and ensuring sufficient steady-state data points for slope determination.

The total internal dimensions of each compartment were measured to calculate the exact gas volume, enabling conversion of GC peak areas to oxygen content. The oxygen content in the

collection chamber was plotted as a function of time, and the slope of the linear regression (steady-state region) was used to calculate the volumetric OTR. The obtained values were corrected for background leakage determined in blank tests and scaled using the results from a reference control film. OTR values were expressed in $cm^3\ m^{-2}h^{-1}$ and all analyses were performed in triplicate.

2.7 | Antimicrobial Testing

2.7.1 | Disk Diffusion Assay

The antibacterial activity of the films was evaluated against common foodborne bacterial pathogens, including *Pseudomonas aeruginosa*, *Listeria monocytogenes*, *Staphylococcus aureus*, *Morganella morganii*, *Salmonella enterica* sv. Typhimurium, *Enterococcus faecalis*, *Escherichia coli*, and *Klebsiella pneumoniae*. The disk diffusion assay was employed according to the Kirby-Bauer protocol [59]. Film samples were cut into 11.8 mm diameter discs, treated for 10 min with CAP using the previously described plasma jet system (Ar, 4 L/min, 10 min), and placed onto Mueller–Hinton agar (MHA) plates that had been pre-inoculated with bacterial suspensions adjusted to 10^7–10^8 CFU mL^{-1} (based on McFarland standards). Plates were incubated at 25°C for 24 h. Untreated film discs were used as controls. No visible inhibition zones were detected for any of the treated films under the tested conditions. All tests were performed in triplicates.

2.7.2 | Shelf-Life Study

A shelf-life study was carried out to assess the potential antimicrobial effect of CAP-treated films in real food conditions via microbial analysis and according to standard protocols [60, 61]. Fresh meager (*Argyrosomus regius*) slices were placed in sterile Petri dishes and wrapped in CAP-treated films, being in direct contact with the fish surface (CAP treatment conditions: Ar, 4 L/min, 10 min). Untreated LDPE and HDPE films were also used for the packaging of the fresh fish slices and served as control samples for comparison to the CAP-treated films. The samples were stored at 2°C ± 0.5°C for a total duration of 13 days.

For the determination of the microbial load, 10 g of fish tissue were aseptically homogenized with 90 mL of sterile Ringer's solution and serial decimal dilutions were prepared and plated on Plate Count Agar (PCA) for the determination of aerobic Total Viable Count (TVC). The incubation was carried out at 25°C for 48 h, a temperature that allows the growth of psychrotrophic populations relevant to chilled fish and thus provides a more representative assessment of the spoilage microbiota. The microbial counts were calculated using the following equation: [62]

$$N = \frac{\sum C}{V \times 1.1 \times d} \tag{8}$$

where N is the number of microorganisms per gram (CFU/g), ΣC is the total number of colonies counted on the two selected plates originating from two consecutive dilutions (with at least one plate containing a minimum of 10 colonies), V is the volume of the inoculum applied to each plate (mL), and d is the dilution factor of the first of the two retained dilutions (with $d = 1$ for undiluted samples). The results were finally expressed as mean $\log_{10}$ (CFU g^{-1}) values.

All analyses were performed in duplicate. The microbial growth was described using the Baranyi growth model and for curve fitting, the program DMFit was used (available at https://www.combase.cc) [63].

2.8 | Degradation Test

The degradation behavior of LDPE and HDPE films was evaluated under controlled soil burial conditions following some of the principles of ASTM D5988-18 standard, with modifications including preliminary sterilization, fungal biofilm pre-incubation and quantification of degradation via residual weight loss (WL) rather than CO_2 evolution [64]. For the pre-incubation, *Aspergillus flavus* was used. Samples (2.5 × 5 cm) were sterilized in 70% ethanol, rinsed with sterile deionized water, oven-dried (50°C, 24 h), and weighed using an analytical balance (±0.0001 g). Four treatment groups were examined for each PE film (LDPE and HDPE): untreated (control), samples treated with CAP, samples pre-incubated with *A. flavus*, and samples subjected to both CAP and fungal pre-incubation.

Plasma treatment was carried out using the previously described plasma jet system (Ar, 4 L/min, 10 min). For fungal inoculation, samples were pre-incubated for 7 days on solid Malt Extract Agar (MEA) medium inoculated with *A. flavus* (10^5 spores mL^{-1}) to allow biofilm formation prior to soil burial (Figure 2).

The test materials were buried at a 10 cm depth in sterile, sieved soil (pH 6.5–7.0, moisture 30%–35%) contained in 1.5 L sealed glass containers and incubated at 25°C ± 4°C for a period of 24 months in total. At selected time points, samples were retrieved (in duplicates), gently cleaned, dried, and reweighed. Degradation was quantified by calculating the percentage of WL using the equation:

$$\mathrm{WL}\,(\%) = \frac{W_0 - W_f}{W_0} \times 100 \tag{9}$$

where W_0 is the initial dry weight of the film, and W_f is the final dry weight of the film retrieved from soil at each time interval.

Surface hydrophilicity was also monitored during degradation through static WCA measurements ($n = 10$), following the same procedure described previously for WCA, in order to assess the weathering state of the plastic samples [65].

2.9 | Statistical Analysis

Statistical analysis was performed by one-way analysis of variance at a 95% confidence interval using Stata 19 software (StataCorp. 2025. Stata Statistical Software: Release19. College

Station, TX: StataCorp LLC.) for the analysis of WVP ($n = 7$), OTR ($n = 3$), WCA ($n = 20$), WCA of degradation ($n = 10$) and %WL ($n = 2$). Significant differences were determined by Tukey's HSD multiple range test ($p < 0.05$). Results were expressed as mean ± standard deviation.

3 | Results

3.1 | Surface Chemistry Characterization

As seen in Figures 3 and 4, the spectra of both materials exhibit strong similarities, particularly the four well-defined characteristic peaks associated with PE hydrocarbon backbone [66]. More specifically, the bands at ~2915 and ~2848 cm^{-1} correspond to the asymmetric and symmetric C–H stretching vibrations of methylene ($–CH_2–$) groups, respectively. Split bands in the regions 1472–1462 and 735–719 cm^{-1} can be attributed to the C–H scissoring vibrations and the C–C rocking modes in $–(CH_2)_n–$ sequences, respectively [67–69]. In both LDPE and HDPE, the appearance of new absorption bands following CAP treatment was observed, consistent with previous FTIR studies on plasma-induced chemical modifications of PE and PP surfaces [67, 68, 70]. In LDPE, both 10- and 30-min treatments led to the emergence of two weak peaks between 3600 and 3200 cm^{-1}, specifically at 3395 and 3190 cm^{-1}. These bands are attributed to O–H stretching vibrations, indicating the formation of hydroxyl groups as a result of plasma exposure [67, 70, 71]. Additionally, a band at ~1645 cm^{-1}, also present in the untreated sample, showed increased intensity after CAP treatment. This band is commonly associated with carbonyl (C═O) and/or C═C stretching vibrations [5, 68, 70, 72]. A distinct reduction in intensity at ~1470 cm^{-1}, accompanied by a simultaneous increase at 1462 cm^{-1}, was observed following CAP treatment in LDPE. This shift may indicate changes in the degree of crystallinity of the polymer [32]. In the case of HDPE, only the 30 min CAP resulted in notable chemical changes. The 10 min treatment did not appear to significantly affect the surface chemistry. In the FTIR spectra of the 30 min treated HDPE, weak bands at ~3395 and ~3185 cm^{-1} were detected, indicative of hydroxyl group formation. A sharp peak at 1646 cm^{-1}, attributed to carbonyl (C═O) stretching, was also

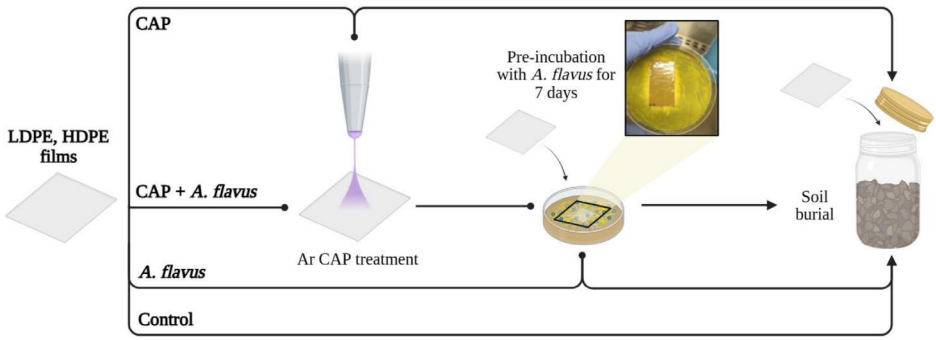

FIGURE 2 | Experimental procedure for the evaluation of the degradation of LDPE and HDPE samples. [Color figure can be viewed at wileyonlinelibrary.com]

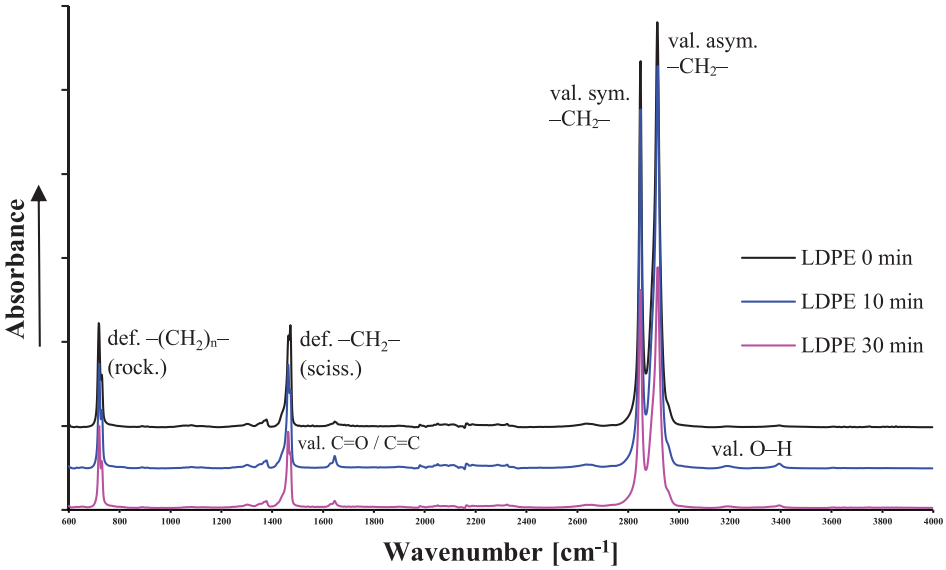

FIGURE 3 | FTIR spectrum of untreated and treated LDPE films. Characteristic peaks corresponding to C–H stretching (around 2915 and 2848 cm^{-1}), C–H scissoring (1472–1462 cm^{-1}), C–C rocking (735–719 cm^{-1}), and other functional groups are indicated. [Color figure can be viewed at wileyonlinelibrary.com]

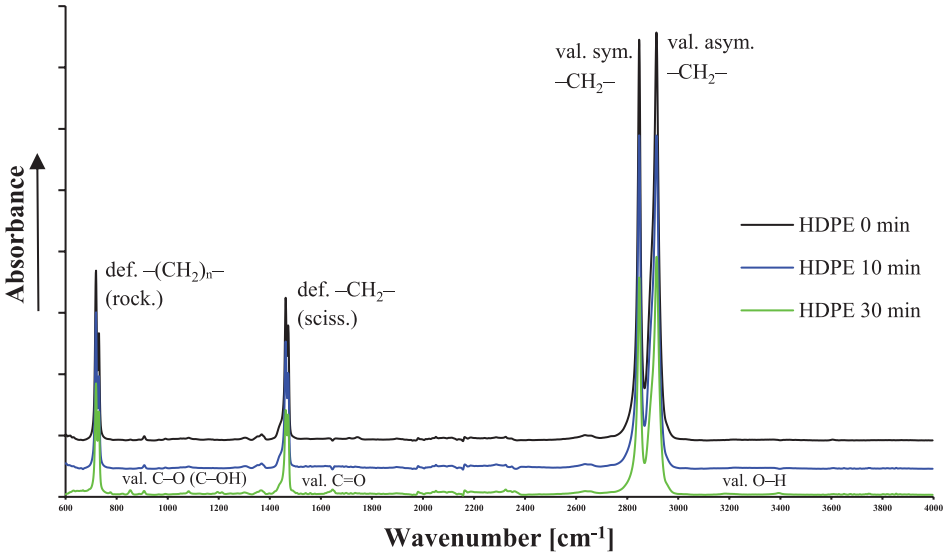

FIGURE 4 | FTIR spectrum of untreated and treated HDPE films. Characteristic peaks corresponding to C–H stretching (around 2915 and 2848 cm^{-1}), C–H scissoring (1472–1462 cm^{-1}), C–C rocking (735–719 cm^{-1}), and other functional groups are indicated. [Color figure can be viewed at wileyonlinelibrary.com]

observed [71]. Moreover, several new bands were detected exclusively in the 30 min treated HDPE, including peaks at 1212 and 1195 cm^{-1}, as well as sharp bands at 1082 and 854 cm^{-1}, which can be assigned to C–O stretching vibrations in C–OH groups [5, 67, 69, 73–75]. Additionally, reductions in the relative intensities at 1462 and 719 cm^{-1} were observed, affecting the 1470/1462 and 729/719 cm^{-1} peak intensity ratios, both of which are indicative of changes in crystallinity. In both materials, a noticeable decrease in the absorbance of the main C–H stretching peaks (~2915 and ~2848 cm^{-1}) was recorded following plasma treatment. This reduction suggests a decreased availability of the corresponding chemical bonds on the surface, likely due to plasma-induced surface oxidation and etching [32].

3.2 | Degree of Crystallinity Estimation

Figure 5 shows the deconvolution profiles of LDPE and HDPE films subjected to Ar CAP treatment for 0, 10, and 30 min in the regions 1475–1420 cm^{-1} and 735–715 cm^{-1}. In most cases, the lower-frequency peaks (1462/719 cm^{-1}) exhibited higher normalized intensities compared to the corresponding higher-frequency peaks (1472/729 cm^{-1}), with untreated LDPE being the only exception (Figure 5). This discrepancy yielded an unusually high crystallinity degree (Table 3) compared to literature reports, which typically fall within 30%–50% [76]. The deviation may be attributed to strong overlap with a medium-intensity band near 1467 cm^{-1} associated with the amorphous phase. As reported by Hagemann et al., this band may display marked asymmetry and interfere with the intensity of the 1472 cm^{-1} band, leading to spectral misinterpretation and artificially elevated crystallinity values. To mitigate this effect, a larger area was consistently assigned to the 1462 cm^{-1} band during fitting, under the assumption that the amorphous contribution is embedded near 1467 cm^{-1} [35]. However, a pronounced fitting error was evident only in the untreated LDPE, where the 1472 cm^{-1} band appeared systematically underestimated.

Due to this reason, we consider the values derived from the 735–715 cm^{-1} region to be more reliable, in agreement with previous studies, since the case of the untreated LDPE clearly distorts the results [77, 78]. Overall, a trend was observed whereby samples with higher crystallinity displayed a more balanced intensity between the two sets of peaks [32].

It is also worth mentioning that LDPE typically does not exhibit split peaks at 1472/1462 and 729/719 cm^{-1}, as its lower crystallinity generally prevents such features from emerging. The presence of these spectral features, considering that increasing polyethylene density is directly associated with improved crystallinity, suggests that the material used is of intermediate density with fewer branching chains, which explains the slightly higher initial crystallinity compared to typical low-density grades [79, 80].

Based on the crystallinity degree obtained from the 729/719 cm^{-1} doublet, Ar CAP treatment affected the crystallinity of both HDPE and LDPE samples (Table 3). For HDPE, crystallinity slightly decreased from 69.98% in the untreated sample to 67.07% after 10 min of treatment, but increased markedly to 78.57% after 30 min. The obtained crystallinity values fall well within the typical range reported in the literature (70%–80%), confirming the consistency of the measurement for this polymer type [32]. In LDPE, crystallinity increased from 53.07% in the untreated sample to 61.50% after 10 min, remaining similar at 61.29% after 30 min.

The changes in crystallinity observed in the present study after Ar CAP treatment are consistent with some previous reports, although the effects strongly depend on polymer type, plasma source, and treatment conditions [81]. In LDPE, the slight increase in crystallinity agrees with the findings of Sanchis et al.

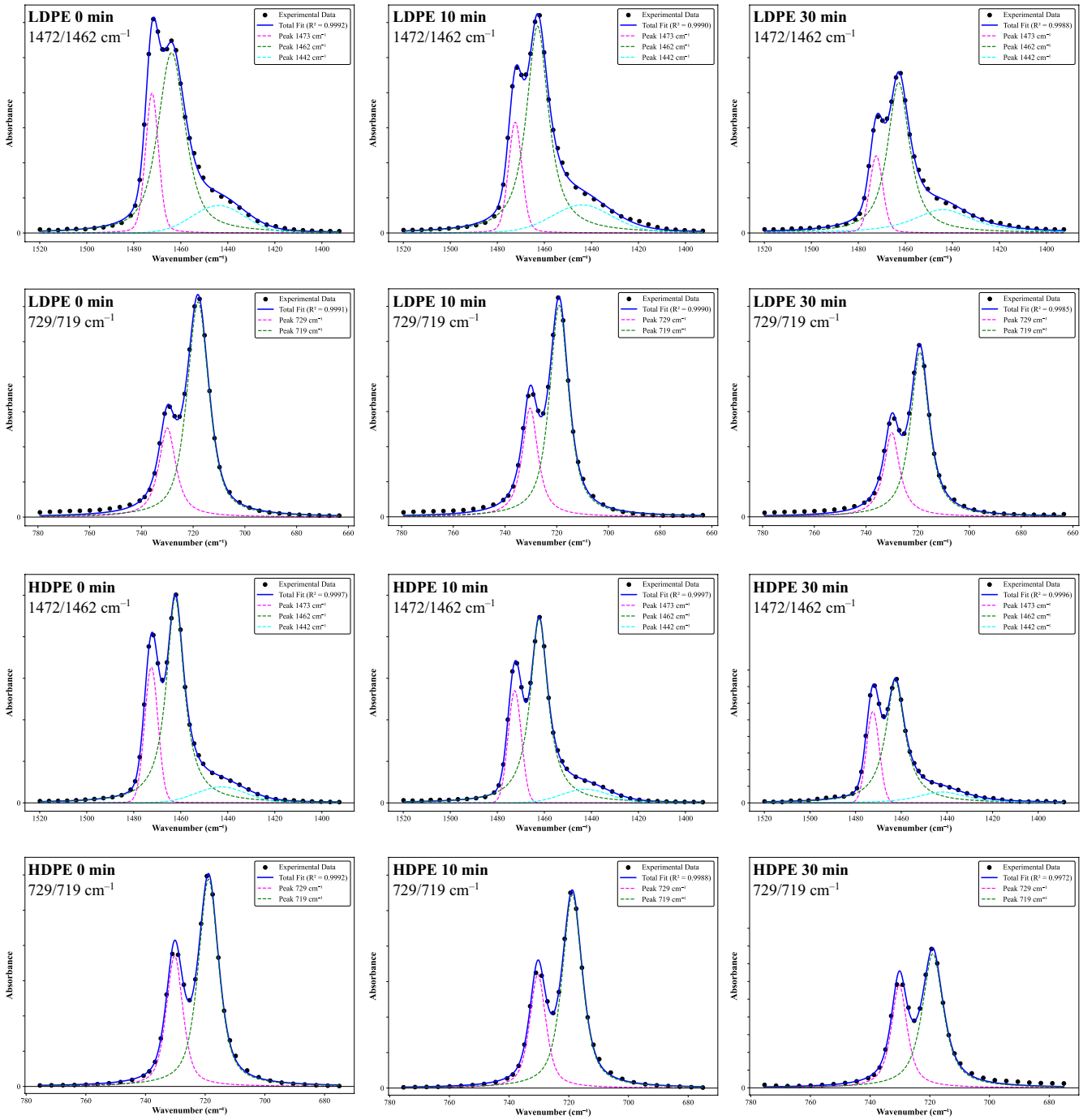

FIGURE 5 | Deconvolution profiles of LDPE and HDPE films at the peaks of 729/719 and 1472/1462 cm^{-1}. [Color figure can be viewed at wileyonlinelibrary.com]

TABLE 3 | Estimated crystallinity degree (%) values of treated and untreated LDPE and HDPE films.

	LDPE			HDPE		
	Control	**10 min**	**30 min**	**Control**	**10 min**	**30 min**
Crystallinity % (peaks 1472/1462 cm^{-1})	79.09	63.14	61.36	72.06	68.58	77.59
Crystallinity % (peaks 729/719 cm^{-1})	53.07	61.50	61.29	69.98	67.07	78.57

who reported a minor enhancement after low-pressure O_2 plasma treatment [14]. Similar phenomena have been reported for other polymers, such as PP and PET, where plasma treatment increases crystallinity and surface roughness due to selective removal of amorphous regions, leaving the crystalline domains unaffected [82, 83]. However, other authors have reported either a decrease

or no effect on polyethylene crystallinity after plasma treatment, which agrees with the 10 min HDPE sample in this study, where the slight decrease -if not attributed to experimental variance- is likely due to crosslinking or temporary structural disruption, and is consistent with the FTIR spectrum showing no distinct differences compared to the control [12, 84, 85]. The disruption of the crystalline order can be attributed to the plasma-induced chain scission and degradation that generates chains with radical tails and increased mobility, facilitating local rearrangements [12]. Moreover, at this stage, the selective removal of the amorphous phase appears not to have yet dominated the surface modification process. In contrast, the marked increase observed after 30 min suggests that with prolonged exposure, the selective etching of the amorphous phase becomes the prevailing mechanism, enriching the surface with crystalline structures. The difference in response between HDPE and LDPE likely reflects their initial crystallinity, as polymers with higher amorphous content are more susceptible to plasma-induced rearrangement [84]. Moreover, Jacobs et al. observed that aging effects are more pronounced in polymers with lower crystallinity, which is consistent with the present results where both LDPE and HDPE showed weaker changes during HR [83].

It is important to interpret these high crystallinity values within the context of the characterization technique. Since ATR-FTIR examines only the surface layer (typically 0.5–2 μm depth), where the plasma impact is mostly intense, the observed increase is attributed to the preferential etching of the amorphous phase, as mentioned before [13, 36, 83]. This selective removal results in a surface layer that is artificially richer in crystalline structures compared to the bulk material; therefore, the reported values reflect the state of the modified surface rather than the volumetric crystallinity of the film. The validity of utilizing ATR-FTIR for such analysis is well-supported in the literature, which confirms that specific IR band doublets are highly sensitive to the conformational order of polymer chains, making the technique a feasible and reliable approach for monitoring relative crystallinity changes in semi-crystalline polymers [31, 32, 66].

3.3 | Surface Morphology Analysis

Figures 6 and 7 displays SEM micrographs at 40,000× magnification for untreated samples and those treated for 10 and 30 min, accompanied by inset images at 100,000× magnification. In both plasma-treated polymers, noticeable surface features were observed, likely associated with the spherulitic organization of polymer chains, indicating that plasma exposure induces significant alterations in the surface morphology, including the formation of prominent grooves and cavities. Such modifications are attributed to the etching action of plasma-generated species (e.g., electrons, ions, free radicals), driven by energetic particle bombardment that simultaneously enhances wettability [5, 18]. Interestingly, HDPE exhibited finer and more angular features in comparison to LDPE. This observation is consistent with previous findings suggesting that plasma preferentially degrades the amorphous regions of PE over the crystalline ones, and as a result, the crystalline domains are more resistant to etching and remain largely intact, giving rise to sharper and smaller structural features [13, 86]. SEM analysis combined with roughness evaluation further showed that the originally smooth topography of the untreated films became irregular and more textured after plasma exposure, a phenomenon also reported in earlier studies [4, 12, 87].

Closer examination of the SEM micrographs after 30 min of plasma treatment revealed distinct differences compared to the 10 min exposure. In the case of HDPE, the surface structures became more numerous, while the larger formations already visible at 10 min not only persisted but also increased in size. In contrast, LDPE displayed a reduced density of surface features,

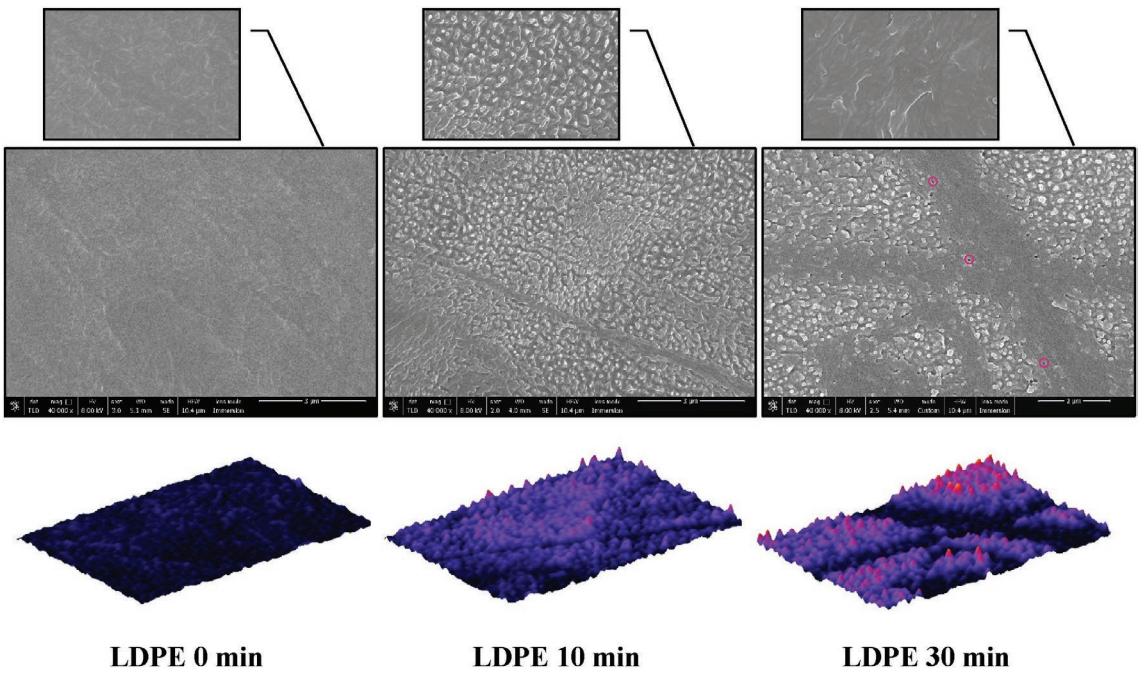

FIGURE 6 | SEM images of untreated and plasma-treated LDPE films at 40,000× magnification, with inset images at 100,000× and corresponding 3D surface plots. [Color figure can be viewed at wileyonlinelibrary.com]

with some areas appearing almost flattened, although the remaining structures also grew in size. Furthermore, pores or well-like depressions were clearly observed in the LDPE surface (highlighted in the corresponding micrograph). These morphological trends can be rationalized by the interplay between etching and smoothing mechanisms: surface protrusions receive a higher flux of reactive species than valleys, which results in their faster removal and a gradual flattening of the topography [88]. At the same time, energy deposition during plasma treatment may progressively shift from the outermost surface to deeper layers, thereby modifying the surface profile and leading to more complex surface geometries [89]. The presence of pores is consistent with previous reports that CP treatment of polyethylene can induce pit and pore formation, while Ar discharges in particular have been shown to produce nanometric holes whose dimensions increase with exposure time [18, 73].

The roughness parameters calculated by image analysis of the 40,000× SEM micrographs (representing a macroscopic roughness scale) are summarized in Table 4. For both polymers, plasma treatment resulted in a marked increase in R_a, R_q, R_p, and R_{max}, accompanied by a decrease in R_v in comparison with the untreated samples. Importantly, after 30 min of treatment the LDPE samples exhibited a slight reduction in overall roughness as well as in R_p, relative to the 10 min samples, whereas R_v decreased further. This trend suggests that surface peaks formed during the initial etching stage were partially flattened, consistent with preferential removal of protrusions by reactive species [88]. A similar evolution was recorded for HDPE, where the roughness values also decreased slightly after 30 min, with R_{max} in particular being reduced compared with 10 min, again pointing to peak flattening.

3.4 | Surface Wettability Measurements

3.4.1 | Hydrophilicity

Figure 8 presents the WCA values for both LDPE and HDPE samples across all plasma treatment durations. The initial WCAs measured for untreated LDPE and HDPE were 98.8° and

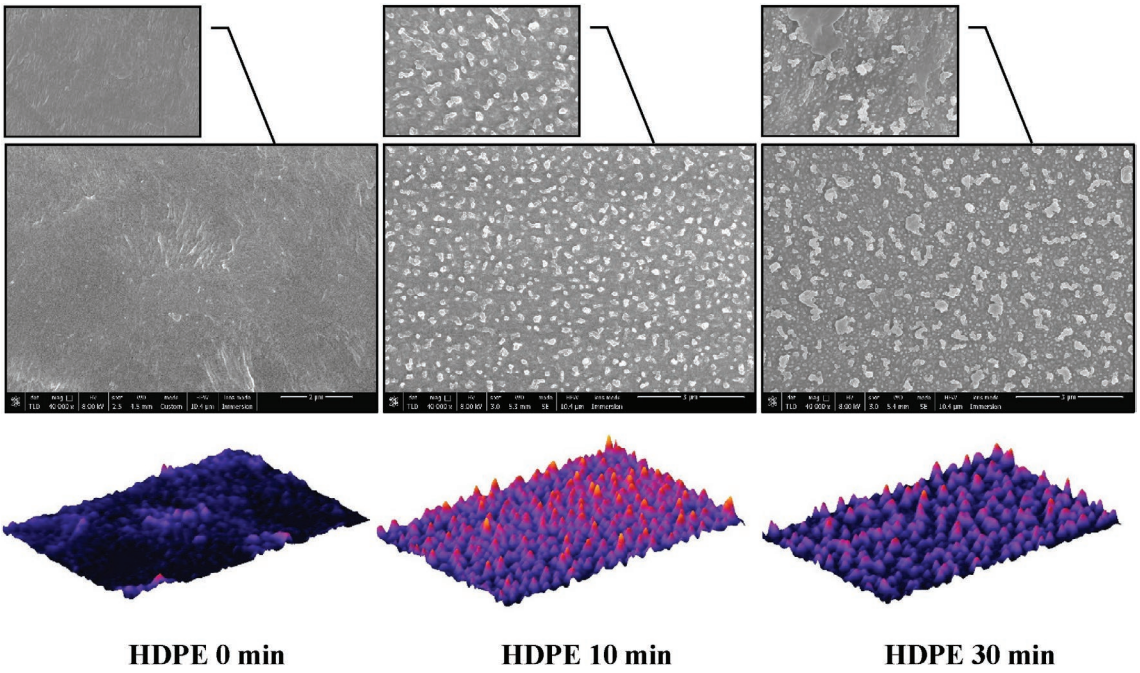

FIGURE 7 | SEM images of untreated and plasma-treated HDPE films at 40,000× magnification, with inset images at 100,000× and corresponding 3D surface plots. [Color figure can be viewed at wileyonlinelibrary.com]

TABLE 4 | Surface roughness parameters (R_a, R_q, R_p, R_v, and R_{max}) of untreated and plasma-treated LDPE and HDPE films, determined from image analysis of 40,000× SEM micrographs.

Sample	R_a (nm)	R_q (nm)	R_v (nm)	R_p (nm)	R_{max} (nm)
LDPE	13.86	11.14	−45.36	52.86	98.23
LDPE 10 min	29.27	22.15	−57.79	110.28	168.08
LDPE 30 min	28.57	21.81	−74.47	100.33	174.80
HDPE	16.72	13.07	−62.84	75.00	137.84
HDPE 10 min	31.25	22.84	−57.18	98.22	155.40
HDPE 30 min	27.52	21.83	−43.10	103.21	146.31

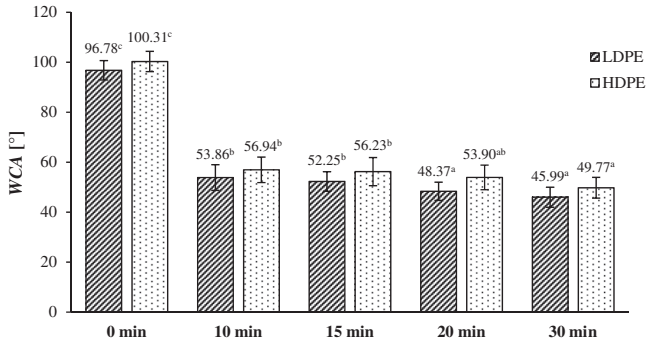

FIGURE 8 | WCA (°) of LDPE and HDPE samples treated with Ar CAP under various durations. Values with different superscripts were significantly different. Different lowercase letters indicate differences between treatment times within the same material group ($n = 20$, $p < 0.05$).

100.31°, respectively, confirming their hydrophobic nature, as contact angles above 90° are typically indicative of hydrophobic surfaces [90, 91]. This limited wettability is characteristic for PE, which is chemically inert and lacks polar functional groups, resulting in low affinity for water and other polar liquids [5]. Following plasma treatment, the WCA of both materials was significantly reduced, nearly by half, in a time-dependent manner. In LDPE, significant reductions were observed after 20 and 30 min of treatment, whereas in HDPE, only the 30 min plasma exposure produced a statistically significant decrease. However, the decrease in contact angle followed a non-linear trend, with the shortest treatment (10 min) resulting in a relatively fast reduction, while subsequent increases in duration yielded only incremental improvements in wettability.

The observed reduction in WCA values aligns with previous studies on Ar plasma-treated PE, where both longer treatment durations and reduced distances from the plasma source – parameters dependent on the specific plasma setup- have been shown to enhance hydrophilic surface modifications [5, 12, 13, 72, 74, 92, 93]. The increase in surface wettability following plasma exposure originates from changes occurring exclusively in the outermost molecular layers of the polymer. Rather than the bulk structure, it is the presence and orientation of surface-exposed functional groups, such as hydroxyl (–OH), carboxyl (–COOH), and carbonyl (C═O), that primarily determine wettability, depending on their ability to minimize interfacial energy and the solid–liquid interface [92]. In addition to chemical modification, changes in surface topography, specifically increased roughness and morphological reorganization, induced by the formation of oxidized groups, also contribute significantly to the observed decrease in contact angle, as demonstrated in studies on plasma-treated PE [18, 22, 94]. Since plasma-induced modifications are limited to the surface, the mobility of polymer chains and the interactions of newly introduced polar groups with ambient humidity can influence the long-term stability of these surface functionalities, potentially resulting in either their stabilization or gradual degradation over time [72].

3.4.2 | Surface Free Energy (SFE)

The SFE of the PE films was calculated using the contact angle measurements of water, diiodomethane, and ethylene glycol.

TABLE 5 | Estimated values of SFE (γ_s) and its components (γ_s^d and γ_s^p) (mJ m^{-2}) of LDPE and HDPE samples.

	γ_s^d (mJ/m^2)	γ_s^p (mJ/m^2)	γ_s (mJ/m^2)
LDPE control	26.12	1.09	27.22
LDPE 10 min	40.79	14.27	55.06
LDPE 15 min	41.73	15.64	57.38
LDPE 20 min	41.73	17.09	58.82
LDPE 30 min	43.21	18.22	61.42
HDPE control	38.15	0.01	38.17
HDPE 10 min	40.79	12.27	53.06
HDPE 15 min	41.73	12.06	53.79
HDPE 20 min	42.32	14.24	56.56
HDPE 30 min	42.47	16.43	58.89

The results for both materials across various plasma treatment durations are presented in Table 5. Untreated LDPE and HDPE films exhibited SFE values of 27.22 and 38.17 mJ m^{-2}, respectively. Following plasma exposure, a progressive increase in SFE was observed, with the highest values recorded after 30 min of treatment (61.42 mJ m^{-2} for LDPE and 58.89 mJ m^{-2} for HDPE). Notably, the variation in SFE values across different treatment times was relatively moderate. These findings confirm that plasma treatment significantly enhances the polar component of surface energy, in agreement with previous reports [12, 13, 95, 96]. The increase of the SFE and the polar components is primarily attributed to the incorporation of polar functional groups such as C–O, C═O, and –OH on the polymer surface. Additionally, morphological changes induced by Ar plasma, specifically surface roughening, facilitate the spreading of test liquids and further contribute to the hydrophilic transformation of the PE surface [72, 92, 97].

3.4.3 | Aging

To evaluate the stability of the hydrophilic surface generated by plasma functionalization, an aging study was conducted over a period of 432 h (18 days) following treatment. Figures 9 and 10 present the evolution of WCA for LDPE and HDPE films treated with plasma for 30 min, monitored as a function of storage time under varying temperature and RH conditions. The data indicate that the majority of the WCA increase, reflecting the HR, occurs within the first 24 h post-treatment. Notably, storage conditions had minimal impact on the recovery behavior, as only slight differences were observed across the tested environments. Over longer storage periods, the rate of WCA increase gradually declines and stabilizes, reaching a plateau between approximately 3 and 6 days, as also reported by Van Deynse et al. [93, 98].

For LDPE and HDPE, the WCA increases from post-treatment averages of 45.99° ± 4.01° and 49.77° ± 4.15°, respectively, to plateau values of 61.81° ± 2.12° for LDPE and 62.98° ± 2.64° for HDPE after storage. The loss of treatment efficiency over time (L%) can be quantified using the following equation:

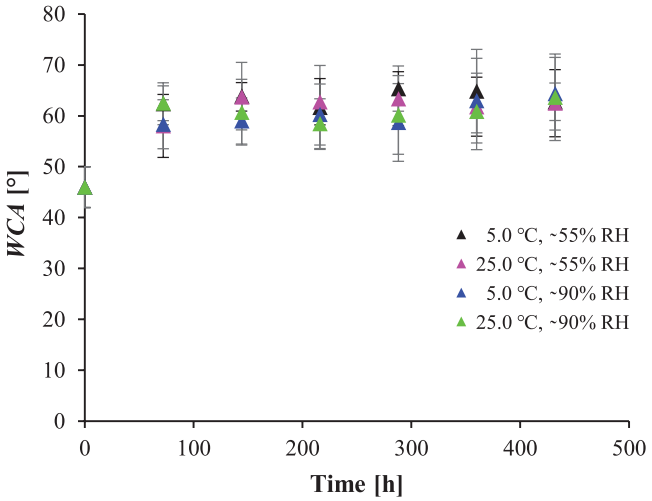

FIGURE 9 | WCA (°) evolution during aging of CAP-treated LDPE for 18 days of storage under various conditions. [Color figure can be viewed at wileyonlinelibrary.com]

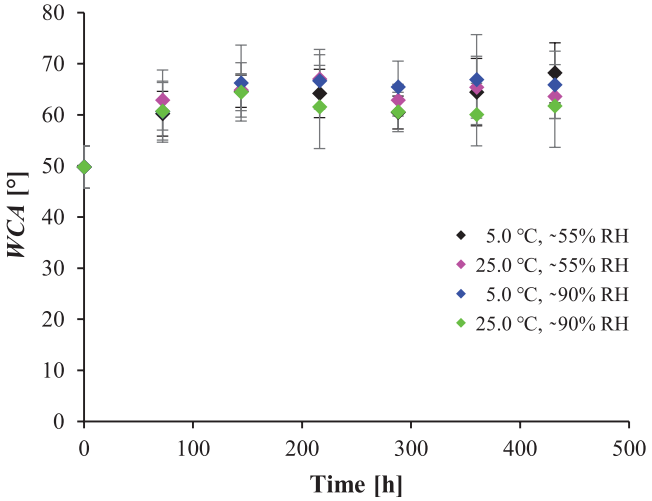

FIGURE 10 | WCA (°) evolution during aging of CAP-treated HDPE for 18 days of storage under various conditions. [Color figure can be viewed at wileyonlinelibrary.com]

$$L\% = 100\frac{\theta_{s1} - \theta_{s2}}{\theta_{s1} - \theta_{untreated}} \quad (10)$$

where θ_{s1} is WCA immediately after plasma treatment (saturation value), θ_{s2} is the plateau value of the WCA value after storage in air and $\theta_{untreated}$ is the WCA value of the untreated material [93]. According to this formula, the treatment efficiency loss ranges from 26% to 30%, indicating that after 18 days of aging, the WCA remains reduced by approximately 36%–37% relative to the untreated state. This suggests that the maximum WCA value reached during the aging process is still significantly lower than those of the untreated materials, reflecting a relatively stable retention of hydrophilic character over time.

This gradual recovery behavior is slower than what has been reported in other studies [86, 98]. It is well established that the overall concentration of oxidized structures does not significantly decrease during aging [13]. Moreover, in polymers where plasma-induced crosslinking has occurred, chain mobility is reduced, leading to slower progression of HR [13, 86, 99]. Given the relatively modest changes in contact angle over time observed for both LDPE and HDPE, it can be inferred that a higher degree of crosslinking may have taken place, thereby restricting the rearrangement of functionalized macromolecular segments [13].

3.5 | Barrier Properties

3.5.1 | Water Vapor Permeability (WVP)

Figure 11 presents the WVP values of both untreated and CAP-treated LDPE and HDPE samples, measured at two temperatures (25°C and 30°C). An increasing trend in WVP was observed with prolonged plasma treatment time for both PE types. In all cases, CAP treatment led to a notable increase in WVP compared to the untreated films. For LDPE at 25°C, a statistically significant difference was observed between 15 and 30 min treatments, whereas at 30°C and in HDPE, the two treatment durations resulted in similar WVP values, indicating no statistically significant difference. Quantitatively, WVP in LDPE doubled at 25°C and increased by approximately 45% at 30°C. For HDPE, the increase was approximately 50% and 60% at 25°C and 30°C, respectively. To the best of our knowledge, no previous study has reported WVP measurements specifically for LDPE and HDPE treated with Ar CAP. However, the present results are consistent with those of Vishnuvarthanan and Rajeswari, who reported an approximately 50% increase in WVTR in PP films following oxygen atmospheric-pressure plasma treatment, and with those of Kim et al. who observed a 16.7%–41.7% increase in the WVP of LDPE, PP, and PET after DBD plasma treatment with atmospheric air. In contrast, other studies have reported that CP treatments with gases such as air, oxygen, or CO_2 generally causes minimal or no changes in water vapor or oxygen permeability in various polymers [81, 100, 101]. The observed increase in WVP after Ar plasma treatment may be explained by considering the underlying mechanisms of vapor transport in polymers. Unlike water absorption, which is a solubility-driven equilibrium process, WVP depends on concentration gradients and vapor pressure differences across the film. This process is controlled by both diffusion and solubility, and is strongly affected by the polymer's structure, crystallinity, free volume, and degree of cross-linking [100, 102, 103]. It is important to note that even polymers with low water absorption, such as silicones or acrylates, can exhibit high WVP due to their structurally open networks [103]. Similarly, in this study, the plasma-induced surface roughening and etching effects from Ar treatment may have resulted in a more open polymer matrix of the outermost layers of the film, thereby facilitating vapor transport. Unlike reactive gases (e.g., O_2, N_2), which induce significant chemical functionalization, inert gases such as Ar or helium mainly produce topographical changes, by breaking C–C and C–H bonds, minimizing chemical modification, and act through physical etching via atomic collisions [18, 104]. These morphological alterations, along with potential increases in free volume or the formation of surface defects, could plausibly account for the elevated WVP values observed in both LDPE and HDPE films.

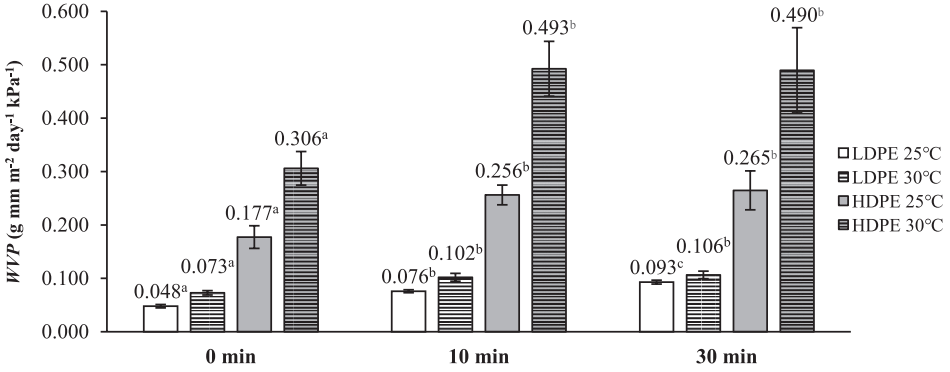

FIGURE 11 | WVP ($g\,mm\,m^{-2}\,day^{-1}\,kPa^{-1}$) of LDPE and HDPE samples measured at 25°C and 30°C. Values with different superscripts were significantly different. Different lowercase letters indicate differences between treatment times within the same material group at each tested temperature ($n = 7$, $p < 0.05$).

From an application perspective, minimizing WVP is typically desired to prevent food dehydration, while the observed increase (up to ~60%) represents a compromise of the barrier function due to surface etching. However, considering the intended application for fresh fish packaging, this trade-off is acceptable for several reasons. First, plasma treatment primarily serves as a surface activation step to enhance adhesion for subsequent functional coatings (e.g., antimicrobial layers), which can seal surface defects and restore or even improve barrier performance, and to also improve printability on the outer package surface [4, 5, 7–11]. Second, for fresh produce, preventing moisture condensation inside the package is crucial; therefore the enhanced hydrophilicity (which can provide an anti-fogging effect) and the slightly increased permeability can help reduce condensation issues without causing rapid product dehydration within the short shelf-life of fresh fish [105]. Finally, despite the relative increase, the modified films retain their bulk structural integrity and do not become porous membranes, maintaining sufficient barrier properties compared to hydrophilic alternatives, such as biopolymers [106].

3.5.2 | Oxygen Transmission Rate (OTR)

The results of the OTR measurements are shown in Figure 12. Only the 30 min treatments were assessed, as they represented the highest-intensity exposures, enabling the evaluation of maximum effects on permeability. After 30 min of Ar plasma exposure, LDPE and HDPE exhibited OTR increases of 45.7% and 10.9%, respectively; however, the increase was substantial and statistically significant only for LDPE. Comparable studies are limited. Rossi et al. examined the gas permeabilities (O_2, CO_2, and N_2) of LDPE and HDPE after Ar plasma treatment and reported considerable reductions, with OTR values remaining stable over 7 days before reaching a steady-state plateau [107]. These effects were attributed to increased cross-linking, with LDPE showing greater susceptibility due to its larger amorphous regions. These findings are not in agreement with the present results. Conversely, Vishnuvarthanan and Rajeswari reported an increase in the OTR of PP following O_2 plasma treatments, with longer exposure times and higher intensities leading to greater permeability, an effect attributed to surface etching and degradation processes [100].

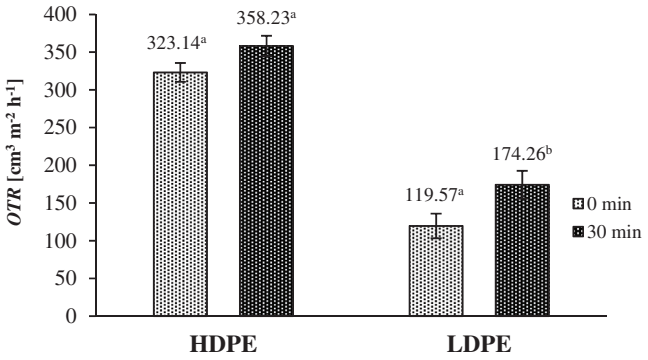

FIGURE 12 | OTR ($cm^3\,m^{-2}\,h^{-1}$) of 30 min-treated and untreated LDPE and HDPE samples. Values with different superscripts were significantly different. Different lowercase letters indicate differences between treatment times within the same material group ($n = 3$, $p < 0.05$).

Although Ar plasma is generally considered effective in promoting cross-linking and thereby enhancing barrier properties, our results indicate a different dominant mechanism under the specific conditions of the APPJ [23, 107]. The pronounced increase in both WVP and OTR suggests that the physical etching effect due to the heavy Ar ions collisions outweighed the benefits of cross-linking [17, 18, 108]. As evidenced by the SEM analysis (Figures 6 and 7), the treatment created significant surface irregularities, grooves, and nanometric defects that likely facilitated vapor and gas diffusion pathways. It is important to distinguish here between bulk intrinsic permeability and the overall transmission rate of the film system. While plasma treatment is surface-limited, the pronounced etching creates morphological alterations that appear to have compromised the integrity of the polymer's dense outer layer ("skin"), thereby facilitating permeation despite the unmodified bulk core [5]. This destruction of the surface boundary layer likely reduced the local effective thickness and lowered the interfacial resistance to mass transfer, thereby facilitating the sorption and subsequent diffusion of permeants through the matrix, despite the unmodified bulk core. This observation is consistent with Vishnuvarthanan and Rajeswari, who similarly attributed increased permeability to plasma-induced surface erosion [100].

3.6 | Antimicrobial Testing

3.6.1 | Shelf-Life Study

The TVC of samples packaged with CAP-treated LDPE and HDPE films are presented in Figure 13. Based on the microbial growth curves, no significant differences were observed between the samples packaged with treated and untreated films, indicating that plasma treatment of the packaging material did not result in a measurable extension of the shelf life of the fresh fish slices. Although HDPE films treated with CAP exhibited slightly lower TVC counts on days 3 and 6, this difference was not sufficient to impact the overall shelf life. The lack of significant antimicrobial effect when plasma-treated films were placed in direct contact with the fish surface can be attributed to two main factors. First CAP-treated packaging films are generally reported to exhibit antimicrobial properties only when further functionalized with bioactive agents or antimicrobial coatings. Second, in the present study, only the packaging films were exposed to plasma, while the food matrix itself was not treated. The microbial inactivation typically associated with CAP arises from the direct interaction of reactive oxygen and nitrogen species (ROS/RNS), along with other short-lived reactive species, with microbial cells present on the food surface [1, 2, 106, 109]. In contrast, while plasma-treated films may exhibit initial sterility, they typically fail to provide sustained antimicrobial activity upon application to food, as the reactive species generated during plasma exposure are highly transient and degrade rapidly, often before they can interact meaningfully with surface microorganisms [1]. Therefore, the absence of antimicrobial activity observed in this study is consistent with the literature and highlights the importance of direct plasma exposure or in-package plasma treatment to achieving effective microbial inactivation and shelf life extension in highly perishable foods such as fish [110, 111].

3.7 | Degradation Test

The degradation behavior of LDPE and HDPE films was evaluated under soil burial conditions using residual WL and changes in surface hydrophilicity (WCA) as indicators. Although polyethylene is highly resistant to biodegradation due to its hydrophobicity and high molecular weight, fungal strains such as *Aspergillus flavus* have demonstrated potential in degrading polyolefins [112–114]. In this study, CAP pretreatment was employed to introduce oxygen-containing groups and increase wettability, aiming to facilitate microbial colonization and enhance the degradation efficiency of *A. flavus* [73, 115]. Previous reports have shown that plasma or UV-based pretreatments can accelerate subsequent microbial degradation of PE, with improvements in WCA reduction and surface roughness being key markers of this effect [116–118].

3.7.1 | Weight Loss (WL)

In this study, LDPE films showed negligible WL under most conditions, with only the combined CAP + *A. flavus* treatment producing measurable degradation after 14, 19, and 24 months (M) ($0.080\% \pm 0.016\%^{a}$, $1.120\% \pm 0.207\%^{a}$, and $1.325\% \pm 0.135\%^{a}$, respectively). Importantly, no WL was detected immediately after CAP treatment in either LDPE or HDPE films, indicating that plasma exposure did not directly cause mass loss but rather acted as a pretreatment influencing subsequent degradation. These values represented the first statistically significant evidence of degradation, yet overall remained modest. Similar absence of significant degradation by *A. flavus* alone was reported by Koutny et al. whereas higher WL has often been documented in liquid media or powdered PE substrates where surface exposure to microbial activity is enhanced [119–124]. Thus, differences in substrate morphology and incubation environment strongly influence outcomes. HDPE films, by contrast, exhibited more pronounced WL (Figure 14). Progressive weight reduction was first detected after 8 M, and the overall trend followed CAP + *A. flavus*>CAP > *A. flavus*. Maximum WL after 24 M reached $8.292\% \pm 2.315\%$, $4.023\% \pm 0.372\%$, and $2.479\% \pm 0.216\%$ for the respective conditions, with statistically significant differences between CAP + *A. flavus* and *A. flavus* alone. Although these values remain lower than those reported in other soil or liquid degradation studies, they nevertheless provide evidence

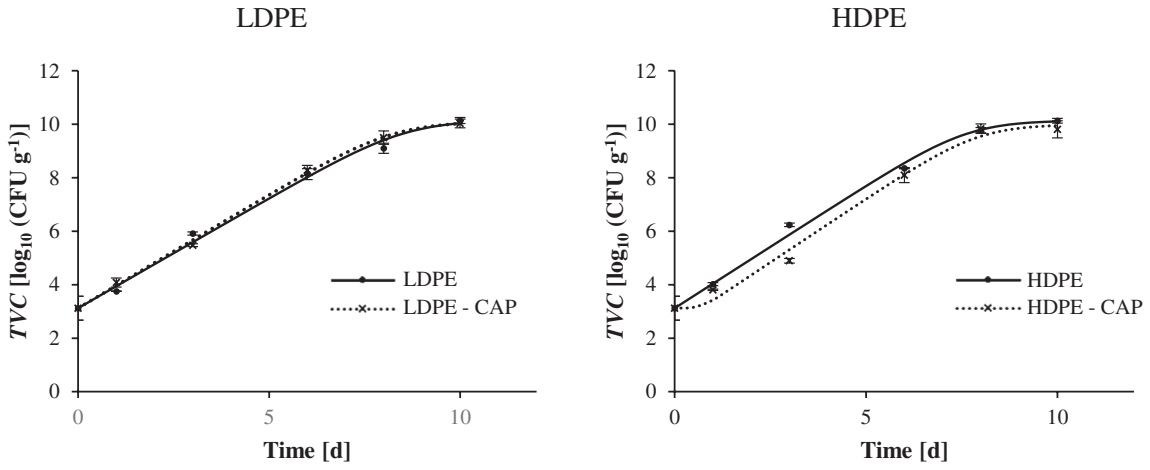

FIGURE 13 | TVC of fish samples packaged with CAP-treated LDPE and HDPE films.

that CAP pretreatment facilitated microbial colonization and accelerated degradation kinetics [73, 125].

3.7.2 | Surface Hydrophilicity

The evolution of WCA values during the soil burial tests is presented in Figure 15. WCA measurements provided additional insight into the degradation behavior, indicating surface modifications consistent with microbial and plasma effects, although WL results were limited for LDPE. Control samples showed only limited reductions over 24 M (HDPE: 100.31° ± 4.06° to 81.46° ± 6.91°, LDPE: 96.78° ± 3.89° to 86.23° ± 8.31°), whereas all other conditions resulted in earlier and more pronounced decreases, with CAP and CAP + *A. flavus* conditions displaying the lowest final WCA values. Decreased WCA indicates increased surface hydrophilicity, reflecting changes in the polymer surface properties.

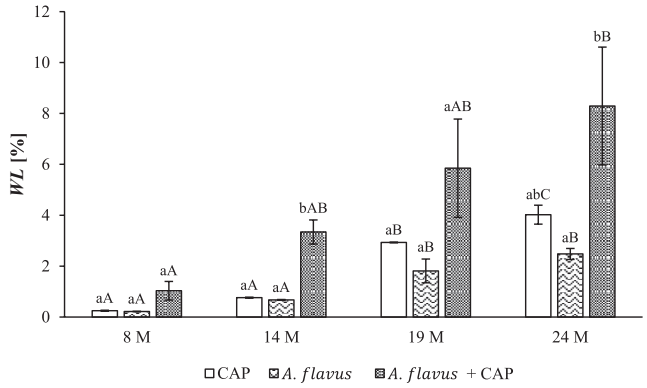

FIGURE 14 | WL (%) of HDPE samples during degradation. Values with different superscripts were significantly different. Different lowercase letters indicate differences between degradation conditions at each tested time interval, while uppercase letters indicate differences within the same degradation condition over different tested time intervals ($n = 2$, $p < 0.05$). Additionally, untreated control samples exhibited negligible WL and are not plotted for clarity.

4 | Conclusions

The results of this study demonstrate that Ar CAP treatment is an effective method for tailoring the surface properties of LDPE and HDPE films. Plasma exposure reduced WCA and increased SFE, thereby enhancing hydrophilicity and facilitating interfacial interactions. Chemical analysis confirmed the incorporation of oxygen-containing functional groups, while morphological characterization revealed etching-driven roughness modifications.

Although water vapor and oxygen permeability increased due to plasma-induced structural alterations (etching), a trade-off often necessary to achieve surface activation, and the direct antimicrobial effect was negligible, these results define the operational limits of the treatment. However, the justification for this modification lies in its critical role as an enabling pretreatment, since physical surface modification alone does not replace active antimicrobial agents or barrier layers, but it acts as a necessary precursor for their effective adhesion and application. The overall surface changes indicate improved potential for adhesion, coating compatibility and functionalization, since the significant increase in surface energy is the necessary precursor for the effective adhesion of subsequent active coatings by preventing delamination and improved printability for labeling.

Aging and degradation tests further indicated partial but stable modification of surface characteristics, while the treatment successfully promoted enhanced biodegradation rates in soil, offering a potential end-of-life advantage. Overall, these findings underscore plasma technology as a versatile tool for polymer surface modification, transforming inert polyolefins into reactive substrates. While the treatment inevitably affects the film intrinsic structure, it is essential for enabling interfacial bonding, thus serving applications requiring enhanced adhesion, such as active coatings and multilayer packaging.

As plasma-treated polymer barrier properties remain relatively underexplored, the present work advances the understanding of structure–property relationships and supports the

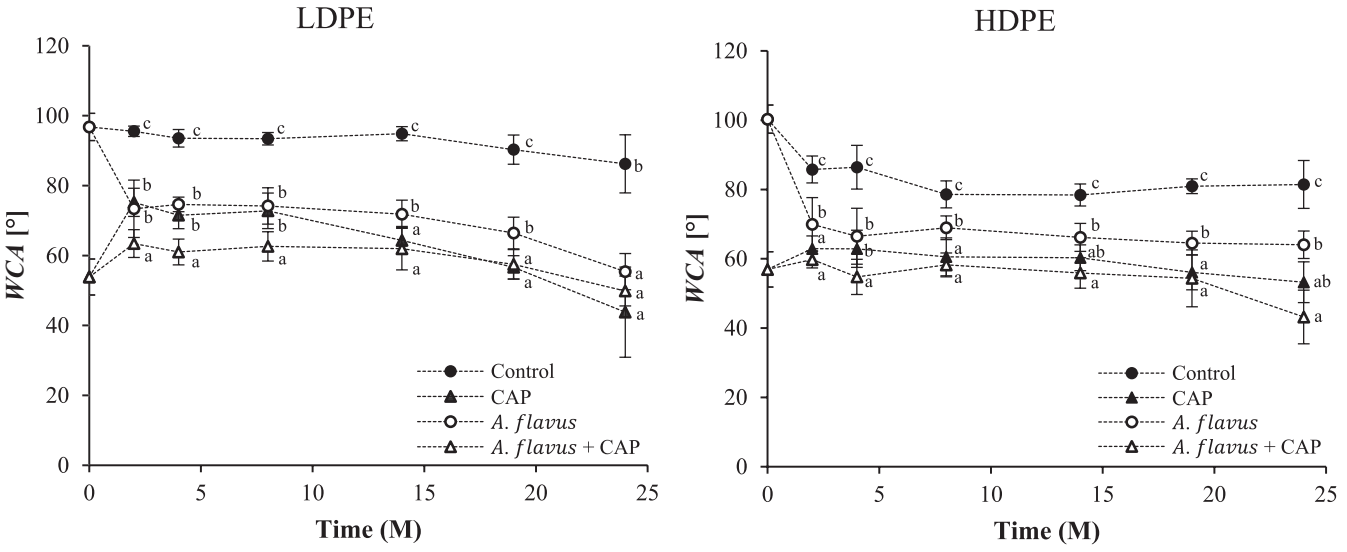

FIGURE 15 | WCA (°) evolution in LDPE and HDPE samples during degradation. Values with different superscripts were significantly different. Different lowercase letters indicate differences between degradation conditions at each tested time interval ($n = 10$, $p < 0.05$).

development of packaging systems with improved interfacial performance. Future research should prioritize optimization of plasma parameters, evaluation of alternative gases and hybrid modification strategies (e.g., plasma-assisted coatings or chemical grafting), and systematic assessment of stability under realistic packaging conditions. In parallel, comprehensive studies of barrier behavior, migration phenomena, toxicological safety assessments and long-term aging and degradation will be essential to evaluate the suitability of plasma-treated polyethylenes (and polyolefins more broadly) in sustainable food packaging applications.

Author Contributions

Aikaterini Spanou: conceptualization (supporting), data curation (lead), formal analysis (lead), investigation (lead), methodology (lead), writing – original draft (lead). **Chrysi Lagkouvardou:** data curation (equal), formal analysis (equal), investigation (equal), writing – review and editing (equal). **Petrina Vogiannou:** data curation (equal), formal analysis (equal), investigation (equal), writing – review and editing (equal). **Vasiliki Korka:** data curation (equal), formal analysis (equal), investigation (equal), writing – review and editing (equal). **Enrico Maurizzi:** formal analysis (equal), investigation (equal), methodology (equal), writing – review and editing (equal). **Ioanna Georgia I. Athanasoulia:** investigation (equal), methodology (equal), validation (equal), writing – review and editing (equal). **Dimitrios Ladakis:** conceptualization (supporting), methodology (equal), supervision (equal), validation (equal), writing – review and editing (equal). **Andrea Pulvirenti:** methodology (equal), resources (equal), supervision (equal), writing – review and editing (equal). **Efstathios Z. Panagou:** methodology (equal), validation (equal), writing – review and editing (equal). **Demetres Briassoulis:** methodology (equal), resources (equal), writing – review and editing (equal). **Apostolis Koutinas:** conceptualization (supporting), methodology (equal), resources (equal), supervision (equal), writing – review and editing (equal). **Theofania Tsironi:** conceptualization (lead), methodology (lead), resources (lead), supervision (lead), validation (lead), writing – review and editing (lead).

Acknowledgments

This study was supported by the Greek Operational Programme for Fisheries, Priority Axis "Innovation in Fisheries," Project title: "Design and development of innova- tive packaging materials with enhanced protective activity for fisheries and from biodegradable materials using fish byproducts (packfish)" (2021–2023) MIS5074718. The research has also received funding from the European Union's Horizon 2020 research and innovation programme under the Marie Sklodowska-Curie Grant Agreement no 872217 (ICHTHYS). The authors gratefully acknowledge Dr. Massimo Tonelli (Centro Interdipartimentale Grandi Strumenti—CIGS, Università di Modena e Reggio Emilia) for acquiring the SEM images and for his valuable technical support. The publication of this article in OA mode was financially supported by HEAL-Link.

Funding

This work was supported by the Greek Operational Programme for Fisheries, Priority Axis "Innovation in Fisheries," Project title: "Design and development of innovative packaging materials with enhanced protective activity for fisheries and from biodegradable materials using fish byproducts (pack4fish)" (2021–2023) MIS5074718, website: http://pack4fish.aua.gr. H2020 Marie Skłodowska-Curie Actions, 872217.

Conflicts of Interest

The authors declare no conflicts of interest.

Data Availability Statement

Data available on request from the corresponding author.

References

1. S. K. Pankaj, C. Bueno-Ferrer, N. N. Misra, et al., "Applications of Cold Plasma Technology in Food Packaging," *Trends in Food Science & Technology* 35, no. 1 (2014): 5–17, https://doi.org/10.1016/j.tifs.2013.10.009.

2. K. Y. Perera, J. Prendeville, A. K. Jaiswal, and S. Jaiswal, "Cold Plasma Technology in Food Packaging," *Coatings* 12, no. 12 (2022): 1896, https://doi.org/10.3390/coatings12121896.

3. C. Mandolfino, E. Lertora, C. Gambaro, and M. Bruno, "Improving Adhesion Performance of Polyethylene Surfaces by Cold Plasma Treatment," *Meccanica* 49, no. 10 (2014): 2299–2306, https://doi.org/10.1007/s11012-014-9993-y.

4. R. M. Sanchis, O. Calvo, L. Sánchez, D. García, and R. Balart, "Enhancement of Wettability in Low Density Polyethylene Films Using Low Pressure Glow Discharge N_2 Plasma," *Journal of Polymer Science, Part B, Polymer Physics* 45, no. 17 (2007): 2390–2399, https://doi.org/10.1002/polb.21246.

5. A. Abusrafa, S. Habib, I. Krupa, M. Ouederni, and A. Popelka, "Modification of Polyethylene by RF Plasma in Different/Mixture Gases," *Coatings* 9, no. 2 (2019): 145, https://doi.org/10.3390/coatings9020145.

6. K. N. Pandiyaraj, A. M. Ferraria, A. M. B. do Rego, et al., "Low-Pressure Plasma Enhanced Immobilization of Chitosan on Low-Density Polyethylene for Bio-Medical Applications," *Applied Surface Science* 328 (2015): 1–12, https://doi.org/10.1016/j.apsusc.2014.12.030.

7. Z. Honarvar, M. Farhoodi, M. R. Khani, et al., "Application of Cold Plasma to Develop Carboxymethyl Cellulose-Coated Polypropylene Films Containing Essential Oil," *Carbohydrate Polymers* 176, no. 1–10 (2017): 1–10, https://doi.org/10.1016/j.carbpol.2017.08.054.

8. P. Lu, M. Guo, Z. Xu, and M. Wu, "Application of Nanofibrillated Cellulose on BOPP/LDPE Film as Oxygen Barrier and Antimicrobial Coating Based on Cold Plasma Treatment," *Coatings* 8, no. 6 (2018): 207, https://doi.org/10.3390/coatings8060207.

9. E. Moradi, M. H. Moosavi, S. M. Hosseini, et al., "Prolonging Shelf Life of Chicken Breast Fillets by Using Plasma-Improved Chitosan/Low Density Polyethylene Bilayer Film Containing Summer Savory Essential Oil," *International Journal of Biological Macromolecules* 156 (2020): 321–328, https://doi.org/10.1016/j.ijbiomac.2020.03.226.

10. L.-W. Wong, X.-J. Loke, C.-K. Chang, W.-C. Ko, C.-Y. Hou, and C.-W. Hsieh, "Use of the Plasma-Treated and Chitosan/Gallic Acid-Coated Polyethylene Film for the Preservation of Tilapia (Orechromis Niloticus) Fillets," *Food Chemistry* 329 (2020): 126989, https://doi.org/10.1016/j.foodchem.2020.126989.

11. B. Yudhistira, A. S. Sulaimana, F. Punthi, et al., "Cold Plasma-Based Fabrication and Characterization of Active Films Containing Different Types of *Myristica fragrans* Essential Oil Emulsion," *Polymers* 14, no. 8 (2022): 1618, https://doi.org/10.3390/polym14081618.

12. M. Ataeefard, S. Moradian, M. Mirabedini, M. Ebrahimi, and S. Asiaban, "Investigating the Effect of Power/Time in the Wettability of Ar and O_2 Gas Plasma-Treated Low-Density Polyethylene," *Progress in Organic Coatings* 64, no. 4 (2009): 482–488, https://doi.org/10.1016/j.porgcoat.2008.08.011.

13. V. Švorčík, K. Kolářová, P. Slepička, A. Macková, M. Novotná, and V. Hnatowicz, "Modification of Surface Properties of High and Low Density Polyethylene by Ar Plasma Discharge," *Polymer Degradation and Stability* 91, no. 6 (2006): 1219–1225, https://doi.org/10.1016/j.polymdegradstab.2005.09.007.

14. M. R. Sanchis, V. Blanes, M. Blanes, D. Garcia, and R. Balart, "Surface Modification of Low Density Polyethylene (LDPE) Film by

Low Pressure O_2 Plasma Treatment," *European Polymer Journal* 42, no. 7 (2006): 1558–1568, https://doi.org/10.1016/j.eurpolymj.2006.02.001.

15. P. Cools, L. Astoreca, P. S. Esbah Tabaei, et al., "Surface Treatment of Polymers by Plasma," in *Surface Modification of Polymers* (Wiley-VCH Verlag GmbH & Co. KGaA, 2019), 31–65, https://doi.org/10.1002/9783527819249.ch2.

16. W. S. Abdul-Majeed, I. M. AL-Handhali, S. H. AL-Yaquobi, and K. O. Al-Riyami, "Application of Novel Polymeric Surface Remediation Technique Based on Flying Jet Plasma Torch," *Industrial & Engineering Chemistry Research* 56, no. 39 (2017): 11352–11358, https://doi.org/10.1021/acs.iecr.7b02729.

17. M. Narimisa, R. Ghobeira, Y. Onyshchenko, N. De Geyter, T. Egghe, and R. Morent, *Different Techniques Used for Plasma Modification of Polyolefin Surfaces* (Springer International Publishing, 2022), 15–56, https://doi.org/10.1007/978-3-030-52264-3_2.

18. S. M. M. Spyrides, F. S. Alencastro, E. F. Guimaraes, F. L. Bastian, and R. A. Simao, "Mechanism of Oxygen and Argon Low Pressure Plasma Etching on Polyethylene (UHMWPE)," *Surface and Coatings Technology* 378 (2019): 124990, https://doi.org/10.1016/j.surfcoat.2019.124990.

19. D. Hegemann, H. Brunner, and C. Oehr, "Plasma Treatment of Polymers for Surface and Adhesion Improvement," *Nuclear Instruments and Methods in Physics Research Section B: Beam Interactions With Materials and Atoms* 208 (2003): 281–286, https://doi.org/10.1016/S0168-583X(03)00644-X.

20. M. Bertin, E. M. Leitao, S. Bickerton, and C. J. R. Verbeek, "A Review of Polymer Surface Modification by Cold Plasmas Toward Bulk Functionalization," *Plasma Processes and Polymers* 21, no. 5 (2024): 2300208, https://doi.org/10.1002/ppap.202300208.

21. T. Felix, V. Soldi, and N. A. Debacher, *Surface Modification and Hydrophobic Recovery (Aging) of Polyolefin Exposed to Plasma* (Springer International Publishing, 2022), 197–214, https://doi.org/10.1007/978-3-030-52264-3_8.

22. S. Tajima and K. Komvopoulos, "Surface Modification of Low-Density Polyethylene by Inductively Coupled Argon Plasma," *Journal of Physical Chemistry B* 109, no. 37 (2005): 17623–17629, https://doi.org/10.1021/jp052121x.

23. Y. Yao, X. Liu, and Y. Zhu, "Surface Modification of High-Density Polyethylene by Plasma Treatment," *Journal of Adhesion Science and Technology* 7, no. 1 (1993): 63–75, https://doi.org/10.1163/156856193X00204.

24. H. Schonhorn and R. H. Hansen, "Surface Treatment of Polymers for Adhesive Bonding," *Journal of Applied Polymer Science* 11, no. 8 (1967): 1461–1474, https://doi.org/10.1002/app.1967.070110809.

25. N. Médard, J.-C. Soutif, and F. Poncin-Epaillard, "Characterization of CO_2 Plasma-Treated Polyethylene Surface Bearing Carboxylic Groups," *Surface and Coatings Technology* 160, no. 2–3 (2002): 197–205, https://doi.org/10.1016/S0257-8972(02)00407-3.

26. M. Mozetič, "Aging of Plasma-Activated Polyethylene and Hydrophobic Recovery of Polyethylene Polymers," *Polymers* 15, no. 24 (2023): 4668, https://doi.org/10.3390/polym15244668.

27. U. Lommatzsch, D. Pasedag, A. Baalmann, G. Ellinghorst, and H.-E. Wagner, "Atmospheric Pressure Plasma Jet Treatment of Polyethylene Surfaces for Adhesion Improvement," *Plasma Processes and Polymers* 4, no. S1 (2007): S1041–S1045, https://doi.org/10.1002/ppap.200732402.

28. K. Polášková, A. Ozkan, M. Klíma, et al., "Comparing Efficiencies of Polypropylene Treatment by Atmospheric Pressure Plasma Jets," *Plasma Processes and Polymers* 20, no. 11 (2023): 2300031, https://doi.org/10.1002/ppap.202300031.

29. X. Fei, S. Kuroda, T. Mori, and K. Hosoi, "High-Density Polyethylene (HDPE) Surface Treatment Using an RF Capacitive Atmospheric Pressure Cold Ar Plasma Jet," *Plasma Science and Technology* 15, no. 6 (2013): 577–581, https://doi.org/10.1088/1009-0630/15/6/16.

30. S. Reuter, T. von Woedtke, and K.-D. Weltmann, "The kINPen—A Review on Physics and Chemistry of the Atmospheric Pressure Plasma Jet and Its Applications," *Journal of Physics D: Applied Physics* 51, no. 23 (2018): 233001, https://doi.org/10.1088/1361-6463/aab3ad.

31. G. Zerbi, G. Gallino, N. Del Fanti, and L. Baini, "Structural Depth Profiling in Polyethylene Films by Multiple Internal Reflection Infra-Red Spectroscopy," *Polymer* 30, no. 12 (1989): 2324–2327, https://doi.org/10.1016/0032-3861(89)90269-3.

32. E. Tarani, I. Arvanitidis, D. Christofilos, D. N. Bikiaris, K. Chrissafis, and G. Vourlias, "Calculation of the Degree of Crystallinity of HDPE/GNPs Nanocomposites by Using Various Experimental Techniques: A Comparative Study," *Journal of Materials Science* 58, no. 4 (2023): 1621–1639, https://doi.org/10.1007/s10853-022-08125-4.

33. K. Tashiro, S. Sasaki, and M. Kobayashi, "Structural Investigation of Orthorhombic-to-Hexagonal Phase Transition in Polyethylene Crystal: The Experimental Confirmation of the Conformationally Disordered Structure by X-Ray Diffraction and Infrared/Raman Spectroscopic Measurements," *Macromolecules* 29, no. 23 (1996): 7460–7469.

34. P. Bernazzani, V. T. Bich, H. Phuong-Nguyen, et al., "FTIR Analysis of the Phase Content in Low-Density Polyethylene," *Canadian Journal of Chemistry* 76, no. 11 (1998): 1674–1687, https://doi.org/10.1139/cjc-76-11-1674.

35. H. Hagemann, R. G. Snyder, A. J. Peacock, and L. Mandelkern, "Quantitative Infrared Methods for the Measurement of Crystallinity and Its Temperature Dependence: Polyethylene," *Macromolecules* 22, no. 9 (1989): 3600–3606, https://doi.org/10.1021/ma00199a017.

36. N. Stavinski, A. Ghasemi, L. J. Bruno, et al., "Real-Time Quantification of Polyethylene Crystallinity via In Situ Mid- and Near-Infrared Correlation Spectroscopy: Melting and Dissolution," *Journal of Polymer Science* 63, no. 10 (2025): 2248–2265, https://doi.org/10.1002/pol.20250207.

37. G. Chinga, P. O. Johnsen, R. Dougherty, E. L. Berli, and J. Walter, "Quantification of the 3D Microstructure of SC Surfaces," *Journal of Microscopy* 227, no. 3 (2007): 254–265, https://doi.org/10.1111/j.1365-2818.2007.01809.x.

38. C. A. Schneider, W. S. Rasband, and K. W. Eliceiri, "NIH Image to ImageJ: 25 Years of Image Analysis," *Nature Methods* 9, no. 7 (2012): 671–675, https://doi.org/10.1038/nmeth.2089.

39. C. Tommasino, C. Sardo, A. Guidone, et al., "Bioinspired PCL-Based Composite Scaffolds Produced via Hot Melt Extrusion and Fused Filament Fabrication: An Integrated Workflow for Enhanced Bone Regeneration," *Journal of Drug Delivery Science and Technology* 106 (2025): 106679, https://doi.org/10.1016/j.jddst.2025.106679.

40. E. S. Gadelmawla, M. M. Koura, T. M. A. Maksoud, I. M. Elewa, and H. H. Soliman, "Roughness Parameters," *Journal of Materials Processing Technology* 123, no. 1 (2002): 133–145, https://doi.org/10.1016/S0924-0136(02)00060-2.

41. "SurfCharJ," n.d., https://www.gcsca.net/IJ/SurfCharJ.html.

42. D. H. Kaelble, "Dispersion-Polar Surface Tension Properties of Organic Solids," *Journal of Adhesion* 2, no. 2 (1970): 66–81, https://doi.org/10.1080/0021846708544582.

43. D. K. Owens and R. C. Wendt, "Estimation of the Surface Free Energy of Polymers," *Journal of Applied Polymer Science* 13, no. 8 (1969): 1741–1747, https://doi.org/10.1002/app.1969.070130815.

44. C. J. van Oss, *Interfacial Forces in Aqueous Media* (CRC Press, 2006), https://doi.org/10.1201/9781420015768.

45. S. Ebnesajjad, *Handbook of Adhesives and Surface Preparation* (Elsevier, 2011), https://doi.org/10.1016/C2010-0-65918-9.

46. S. Ebnesajjad, *Surface Treatment of Materials for Adhesion Bonding* (William Andrew, 2006).

47. D. Manas, M. Bednarik, A. Mizera, M. Manas, M. Ovsik, and P. Stoklasek, "Effect of Beta Radiation on the Quality of the Bonded Joint for Difficult to Bond Polyolefins," *Polymers* 11, no. 11 (2019): 1863, https://doi.org/10.3390/polym11111863.

48. M. Pascual, R. Balart, L. Sánchez, O. Fenollar, and O. Calvo, "Study of the Aging Process of Corona Discharge Plasma Effects on Low Density Polyethylene Film Surface," *Journal of Materials Science* 43, no. 14 (2008): 4901–4909, https://doi.org/10.1007/s10853-008-2712-0.

49. J. Nakamatsu, L. F. Delgado-Aparicio, R. Da Silva, and F. Soberon, "Ageing of Plasma-Treated Poly(Tetrafluoroethylene) Surfaces," *Journal of Adhesion Science and Technology* 13, no. 7 (1999): 753–761, https://doi.org/10.1163/156856199X00983.

50. L. Greenspan, "Humidity Fixed Points of Binary Saturated Aqueous Solutions," *Journal of Research of the National Bureau of Standards Section A: Physics and Chemistry* 81A, no. 1 (1977): 89, https://doi.org/10.6028/jres.081A.011.

51. R. H. Stokes and R. A. Robinson, "Standard Solutions for Humidity Control at 25°C," *Industrial and Engineering Chemistry* 41, no. 9 (1949): 13896–13901, https://doi.org/10.1021/ie50477a041.

52. L. B. Rockland, "Saturated Salt Solutions for Static Control of Relative Humidity Between 5° and 40°C," *Analytical Chemistry* 32, no. 10 (1960): 1375–1376, https://doi.org/10.1021/ac60166a055.

53. A. Wexler and S. Hasegawa, "Relative Humidity-Temperature Relationships of Some Saturated Salt Solutions in the Temperature Range 0° to 50°C," *Journal of Research of the National Bureau of Standards* 53, no. 1 (1954): 19, https://doi.org/10.6028/jres.053.003.

54. ASTM E96/E96M, *ASTM Test Methods for Water Vapor Transmission of Materials* (ASTM International, 2014), https://doi.org/10.1520/E0096_E0096M-14.

55. ASTM E2945, *Test Method for Film Permeability Determination Using Static Permeability Cells* (ASTM International, 2014), https://doi.org/10.1520/E2945-14.

56. S. K. Papiernik, S. R. Yates, and J. Gan, "An Approach for Estimating the Permeability of Agricultural Films," *Environmental Science & Technology* 35, no. 6 (2001): 1240–1246, https://doi.org/10.1021/es0014279.

57. S. K. Papiernik, F. F. Ernst, and S. R. Yates, "An Apparatus for Measuring the Gas Permeability of Films," *Journal of Environmental Quality* 31, no. 1 (2002): 358–361, https://doi.org/10.2134/jeq2002.3580.

58. S. Zeman and L. Kubik, "Evaluation of Oxygen Permeability of Polyethylene Films," *Technical Sciences/University of Warmia and Mazury in Olsztyn* 15, no. 2 (2012): 331–345.

59. J. Hudzicki, "Kirby-Bauer Disk Diffusion Susceptibility Test Protocol," *American Society for Microbiology* (2009): 1–23, https://asm.org/protocols/kirby-bauer-disk-diffusion-susceptibility-test-pro.

60. International Organization for Standardization (ISO), "ISO ISO 4833-1: Microbiology of the Food Chain—Horizontal Method for the Enumeration of Microorganisms—Part 1: Colony Count at 30°C by the Pour Plate Technique," 2013.

61. ICMSF, *Microorganisms in Foods 2: Sampling for Microbiological Analysis: Principles and Specific Applications*, 2nd ed. (Blackwell Scientific Publications, 1986).

62. International Organization for Standardization (ISO), "ISO ISO 7218: Microbiology of Food and Animal Feeding Stuffs—General Requirements and Guidance for Microbiological Examinations," 2007.

63. J. Baranyi, T. A. Roberts, and P. McClure, "A Non-Autonomous Differential Equation to Modelbacterial Growth," *Food Microbiology* 10, no. 1 (1993): 43–59, https://doi.org/10.1006/fmic.1993.1005.

64. ASTM International, *Test Method for Determining Aerobic Biodegradation of Plastic Materials in Soil, ASTM D5988* (ASTM International, 2018), https://doi.org/10.1520/D5988-18.

65. A. Benke, J. Sonnenberg, K. Oelschlägel, M. Schneider, M. Lux, and A. Potthoff, "Wettability After Artificial and Natural Weathering of Polyethylene Terephthalate," *Environments* 9, no. 11 (2022): 134, https://doi.org/10.3390/environments9110134.

66. J. V. Gulmine, P. R. Janissek, H. M. Heise, and L. Akcelrud, "Polyethylene Characterization by FTIR," *Polymer Testing* 21, no. 5 (2002): 557–563, https://doi.org/10.1016/S0142-9418(01)00124-6.

67. N. De Geyter, R. Morent, and C. Leys, "Surface Characterization of Plasma-Modified Polyethylene by Contact Angle Experiments and ATR-FTIR Spectroscopy," *Surface and Interface Analysis* 40, no. 3–4 (2008): 608–611, https://doi.org/10.1002/sia.2611.

68. R. Morent, N. De Geyter, C. Leys, L. Gengembre, and E. Payen, "Comparison Between XPS- and FTIR-Analysis of Plasma-Treated Polypropylene Film Surfaces," *Surface and Interface Analysis* 40, no. 3–4 (2008): 597–600, https://doi.org/10.1002/sia.2619.

69. G. Socrates, *Infrared and Raman Characteristic Group Frequencies: Tables and Charts*, 3rd ed. (John Wiley & Sons, 2004).

70. R. L. Kovács, M. Csontos, S. Gyöngyösi, et al., "Surface Characterization of Plasma-Modified Low Density Polyethylene by Attenuated Total Reflectance Fourier-Transform Infrared (ATR-FTIR) Spectroscopy Combined With Chemometrics," *Polymer Testing* 96 (2021): 107080, https://doi.org/10.1016/j.polymertesting.2021.107080.

71. M. J. D. De Leon and M. R. Vasquez, "Adhesion of Water-Based Paint on Plasma-Treated High-Density Polyethylene Sheets," *Materials Research Express* 8, no. 10 (2021): 105306, https://doi.org/10.1088/2053-1591/ac3164.

72. J. F. d. M. Neto, I. de Alves Souza, M. C. Feitor, et al., "Study of High-Density Polyethylene (HDPE) Kinetics Modification Treated by Dielectric Barrier Discharge (DBD) Plasma," *Polymers* 12, no. 10 (2020): 2422, https://doi.org/10.3390/polym12102422.

73. C. Chen, N. Taghavi, and S. Baroutian, "Effect of Cold Plasma Pretreatment on Biodegradation of High-Density Polyethylene (HDPE) and Polystyrene (PS)," *Journal of Material Cycles and Waste Management* 26, no. 3 (2024): 1596–1608, https://doi.org/10.1007/s10163-024-01913-x.

74. K. G. Kostov, T. M. C. Nishime, A. H. R. Castro, A. Toth, and L. R. O. Hein, "Surface Modification of Polymeric Materials by Cold Atmospheric Plasma Jet," *Applied Surface Science* 314 (2014): 367–375, https://doi.org/10.1016/j.apsusc.2014.07.009.

75. N. Taghavi, W.-Q. Zhuang, and S. Baroutian, "Enhanced Biodegradation of Non-Biodegradable Plastics by UV Radiation: Part 1," *Journal of Environmental Chemical Engineering* 9, no. 6 (2021): 106464, https://doi.org/10.1016/j.jece.2021.106464.

76. P. P. Ndibewu, T. E. Lefakane, and T. E. Netshiozwi, "Effects of Titanium Dioxide (TiO_2) on Physico-Chemical Properties of Low-Density Polyethylene," *Polymers* 16, no. 19 (2024): 2788, https://doi.org/10.3390/polym16192788.

77. M. Hamzah, M. Khenfouch, A. Rjeb, et al., "Surface Chemistry Changes and Microstructure Evaluation of Low Density Nanocluster Polyethylene Under Natural Weathering: A Spectroscopic Investigation," *Journal of Physics: Conference Series* 984 (2018): 12010, https://doi.org/10.1088/1742-6596/984/1/012010.

78. M. Kaci, T. Sadoun, and S. Cimmino, "Crystallinity Measurements of Unstabilized and HALS-Stabilized LDPE Films Exposed to Natural Weathering by FT-IR, DSC and WAXS Analyses," *International Journal of Polymer Analysis and Characterization* 6, no. 5 (2001): 455–464, https://doi.org/10.1080/10236660108033961.

79. B. C. Smith, "The Infrared Spectra of Polymers II: Polyethylene," *Spectroscopy* 36, no. 5 (2021): 24–29, https://doi.org/10.56530/spectroscopy.xp7081p7.

80. D. Li, L. Zhou, X. Wang, L. He, and X. Yang, "Effect of Crystallinity of Polyethylene With Different Densities on Breakdown Strength and Conductance Property," *Materials* 12, no. 11 (2019): 1746, https://doi.org/10.3390/ma12111746.

81. S. K. Pankaj and S. Thomas, "Cold Plasma Applications in Food Packaging," in *Cold Plasma in Food and Agriculture* (Elsevier, 2016), 293–307, https://doi.org/10.1016/B978-0-12-801365-6.00012-3.

82. O. Xosocotla, H. Martinez, and B. Campillo, "Crystallinity and Hardness Enhancement of Polypropylene Using Atmospheric Pressure Plasma Discharge Treatment," *Advances in Science, Technology and Engineering Systems Journal* 5, no. 6 (2020): 1250–1257, https://doi.org/10.25046/aj0506149.

83. T. Jacobs, N. De Geyter, R. Morent, S. Van Vlierberghe, P. Dubruel, and C. Leys, "Plasma Modification of PET Foils With Different Crystallinity," *Surface and Coatings Technology* 205 (2011): S511–S515, https://doi.org/10.1016/j.surfcoat.2011.01.029.

84. P. Chytrosz-Wrobel, M. Golda-Cepa, E. Stodolak-Zych, J. Rysz, and A. Kotarba, "Effect of Oxygen Plasma-Treatment on Surface Functional Groups, Wettability, and Nanotopography Features of Medically Relevant Polymers With Various Crystallinities," *Applied Surface Science Advances* 18 (2023): 100497, https://doi.org/10.1016/j.apsadv.2023.100497.

85. I. Novák, A. Popelka, I. Krupa, et al., "High-Density Polyethylene Functionalized by Cold Plasma and Silanes," *Vacuum* 86, no. 12 (2012): 2089–2094, https://doi.org/10.1016/j.vacuum.2012.04.046.

86. K. S. Kim, C. M. Ryu, C. S. Park, G. S. Sur, and C. E. Park, "Investigation of Crystallinity Effects on the Surface of Oxygen Plasma Treated Low Density Polyethylene Using X-Ray Photoelectron Spectroscopy," *Polymer* 44, no. 20 (2003): 6287–6295, https://doi.org/10.1016/S0032-3861(03)00674-8.

87. M. Lehocký, H. Drnovská, B. Lapčíková, et al., "Plasma Surface Modification of Polyethylene," *Colloids and Surfaces A: Physicochemical and Engineering Aspects* 222, no. 1–3 (2003): 125–131, https://doi.org/10.1016/S0927-7757(03)00242-5.

88. M. Martin and G. Cunge, "Surface Roughness Generated by Plasma Etching Processes of Silicon," *Journal of Vacuum Science & Technology, B: Microelectronics and Nanometer Structures–Processing, Measurement, and Phenomena* 26, no. 4 (2008): 1281–1288, https://doi.org/10.1116/1.2932091.

89. T. Felix, L. Benetoli, S. Sério, M. Dotto, and N. Debacher, "Temporal Evolution of Roughness Development on Polymer Surfaces Exposed to Non-Thermal Plasma," *Journal of the Brazilian Chemical Society* 31, no. 10 (2020): 2012–2022, https://doi.org/10.21577/0103-5053.20200101.

90. A. Jordá-Vilaplana, V. Fombuena, D. García-García, M. D. Samper, and L. Sánchez-Nácher, "Surface Modification of Polylactic Acid (PLA) by Air Atmospheric Plasma Treatment," *European Polymer Journal* 58 (2014): 23–33, https://doi.org/10.1016/j.eurpolymj.2014.06.002.

91. M. Shabbir and M. Kaushik, "Engineered Nanomaterials: Scope in Today's Textile Industry," in *Handbook of Nanomaterials for Manufacturing Applications* (Elsevier, 2020), 249–263, https://doi.org/10.1016/B978-0-12-821381-0.00010-7.

92. K. N. Pandiyaraj, R. R. Deshmukh, I. Ruzybayev, et al., "Influence of Non-Thermal Plasma Forming Gases on Improvement of Surface Properties of Low Density Polyethylene (LDPE)," *Applied Surface Science* 307 (2014): 109–119, https://doi.org/10.1016/j.apsusc.2014.03.177.

93. A. Van Deynse, P. Cools, C. Leys, R. Morent, and N. De Geyter, "Surface Modification of Polyethylene in an Argon Atmospheric Pressure Plasma Jet," *Surface and Coatings Technology* 276 (2015): 384–390, https://doi.org/10.1016/j.surfcoat.2015.06.041.

94. S. M. M. Spyrides, M. do Prado, J. R. de Araujo, R. A. Simão, and F. L. Bastian, "Effects of Plasma on Polyethylene Fiber Surface for Prosthodontic Application," *Journal of Applied Oral Science* 23, no. 6 (2015): 614–622, https://doi.org/10.1590/1678-775720150260.

95. H. Drnovská, L. Lapčík, V. Buršíková, J. Zemek, and A. M. Barros-Timmons, "Surface Properties of Polyethylene After Low-Temperature Plasma Treatment," *Colloid and Polymer Science* 281, no. 11 (2003): 1025–1033, https://doi.org/10.1007/s00396-003-0871-8.

96. L.-S. Shi, L.-Y. Wang, and Y.-N. Wang, "The Investigation of Argon Plasma Surface Modification to Polyethylene: Quantitative ATR-FTIR Spectroscopic Analysis," *European Polymer Journal* 42, no. 7 (2006): 1625–1633, https://doi.org/10.1016/j.eurpolymj.2006.01.007.

97. P. Slepička, N. Slepičková Kasálková, E. Stránská, L. Bačáková, and V. Švorčík, "Surface Characterization of Plasma Treated Polymers for Applications as Biocompatible Carriers," *Express Polymer Letters* 7, no. 6 (2013): 535–545, https://doi.org/10.3144/expresspolymlett.2013.50.

98. A. Van Deynse, P. Cools, C. Leys, R. Morent, and N. De Geyter, "Influence of Ambient Conditions on the Aging Behavior of Plasma-Treated Polyethylene Surfaces," *Surface and Coatings Technology* 258 (2014): 359–367, https://doi.org/10.1016/j.surfcoat.2014.08.073.

99. W. J. Brennan, W. J. Feast, H. S. Munro, and S. A. Walker, "Investigation of the Ageing of Plasma Oxidized PEEK," *Polymer* 32, no. 8 (1991): 1527–1530, https://doi.org/10.1016/0032-3861(91)90436-M.

100. M. Vishnuvarthanan and N. Rajeswari, "Effect of Mechanical, Barrier and Adhesion Properties on Oxygen Plasma Surface Modified PP," *Innovative Food Science & Emerging Technologies* 30 (2015): 119–126, https://doi.org/10.1016/j.ifset.2015.05.007.

101. S. Y. Kim, I. H. Bang, and S. C. Min, "Effects of Packaging Parameters on the Inactivation of Salmonella Contaminating Mixed Vegetables in Plastic Packages Using Atmospheric Dielectric Barrier Discharge Cold Plasma Treatment," *Journal of Food Engineering* 242 (2019): 55–67, https://doi.org/10.1016/j.jfoodeng.2018.08.020.

102. N. Tenn, N. Follain, K. Fatyeyeva, et al., "Improvement of Water Barrier Properties of Poly(Ethylene- *Co* -Vinyl Alcohol) Films by Hydrophobic Plasma Surface Treatments," *Journal of Physical Chemistry C* 116, no. 23 (2012): 12599–12612, https://doi.org/10.1021/jp302223j.

103. C. Chaiwong, P. Rachtanapun, P. Wongchaiya, R. Auras, and D. Boonyawan, "Effect of Plasma Treatment on Hydrophobicity and Barrier Property of Polylactic Acid," *Surface and Coatings Technology* 204, no. 18–19 (2010): 2933–2939, https://doi.org/10.1016/j.surfcoat.2010.02.048.

104. Y. A. Oh, S. H. Roh, and S. C. Min, "Cold Plasma Treatments for Improvement of the Applicability of Defatted Soybean Meal-Based Edible Film in Food Packaging," *Food Hydrocolloids* 58 (2016): 150–159, https://doi.org/10.1016/j.foodhyd.2016.02.022.

105. J. Shi, L. Xu, and D. Qiu, "Effective Antifogging Coating From Hydrophilic/Hydrophobic Polymer Heteronetwork," *Advanced Science* 9, no. 14 (2022): 2200072, https://doi.org/10.1002/advs.202200072.

106. M. Hoque, C. McDonagh, B. K. Tiwari, J. P. Kerry, and S. Pathania, "Effect of Cold Plasma Treatment on the Packaging Properties of Biopolymer-Based Films: A Review," *Applied Sciences* 12, no. 3 (2022): 1346, https://doi.org/10.3390/app12031346.

107. A. Rossi, L. Incarnato, V. Tagliaferri, and D. Acierno, "Modification of Barrier Properties of Polymeric Films of LDPE and HDPE by Cold Plasma Treatment," *Journal of Polymer Engineering* 14 (1995): 2–3, https://doi.org/10.1515/POLYENG.1995.14.2-3.191.

108. B. Jaleh, B. F. Mohazzab, A. Moradi, and B. F. Mohazzab, *Plasma Modified Polyolefine: Physical Changing and Applications* (Springer International Publishing, 2022), 57–90, https://doi.org/10.1007/978-3-030-52264-3_3.

109. N. N. Misra, B. K. Tiwari, K. S. M. S. Raghavarao, and P. J. Cullen, "Nonthermal Plasma Inactivation of Food-Borne Pathogens," *Food*

Engineering Reviews 3, no. 3–4 (2011): 159–170, https://doi.org/10.1007/s12393-011-9041-9.

110. R. Alaguthevar, J. S. Packialakshmi, B. Murugesan, J. Rhim, and U. Thiyagamoorthy, "In-Package Cold Plasma Treatment to Extend the Shelf Life of Food," *Comprehensive Reviews in Food Science and Food Safety* 23, no. 2 (2024): 13318, https://doi.org/10.1111/1541-4337.13318.

111. D. Ziuzina, S. Patil, P. J. Cullen, K. M. Keener, and P. Bourke, "Atmospheric Cold Plasma Inactivation of *Escherichia coli* in Liquid Media Inside a Sealed Package," *Journal of Applied Microbiology* 114, no. 3 (2013): 778–787, https://doi.org/10.1111/jam.12087.

112. S. Ghatge, Y. Yang, J.-H. Ahn, and H.-G. Hur, "Biodegradation of Polyethylene: A Brief Review," *Applied Biological Chemistry* 63, no. 1 (2020): 27, https://doi.org/10.1186/s13765-020-00511-3.

113. M. K. Sangale, M. Shahnawaz, and A. B. Ade, "Potential of Fungi Isolated From the Dumping Sites Mangrove Rhizosphere Soil to Degrade Polythene," *Scientific Reports* 9, no. 1 (2019): 5390, https://doi.org/10.1038/s41598-019-41448-y.

114. M. Srikanth, T. S. R. S. Sandeep, K. Sucharitha, and S. Godi, "Biodegradation of Plastic Polymers by Fungi: A Brief Review," *Bioresources and Bioprocessing* 9, no. 1 (2022): 42, https://doi.org/10.1186/s40643-022-00532-4.

115. K. Bule Možar, M. Miloloža, V. Martinjak, et al., "Potential of Advanced Oxidation as Pretreatment for Microplastics Biodegradation," *Separations* 10, no. 2 (2023): 132, https://doi.org/10.3390/separations10020132.

116. A. Esmaeili, A. A. Pourbabaee, H. A. Alikhani, F. Shabani, and E. Esmaeili, "Biodegradation of Low-Density Polyethylene (LDPE) by Mixed Culture of *Lysinibacillus xylanilyticus* and *Aspergillus niger* in Soil," *PLoS One* 8, no. 9 (2013): e71720, https://doi.org/10.1371/journal.pone.0071720.

117. L. D. Gómez-Méndez, D. A. Moreno-Bayona, R. A. Poutou-Piñales, et al., "Biodeterioration of Plasma Pretreated LDPE Sheets by *Pleurotus ostreatus*," *PLoS One* 13, no. 9 (2018): e0203786, https://doi.org/10.1371/journal.pone.0203786.

118. L. Scally, M. Gulan, L. Weigang, P. J. Cullen, and V. Milosavljevic, "Significance of a Non-Thermal Plasma Treatment on LDPE Biodegradation With *Pseudomonas aeruginosa*," *Materials* 11, no. 10 (2018): 1925, https://doi.org/10.3390/ma11101925.

119. S. Abdullah, L. Maroof, M. Iqbal, S. Farman, Lubna, and S. Faisal, "Biodegradation of Low-Density Polyethylene (LDPE) Bags by Fungi Isolated From Waste Disposal Soil," *Applied and Environmental Soil Science* 2022 (2022): 1–7, https://doi.org/10.1155/2022/8286344.

120. G. C. DSouza, R. S. Sheriff, V. Ullanat, et al., "Fungal Biodegradation of Low-Density Polyethylene Using Consortium of Aspergillus Species Under Controlled Conditions," *Heliyon* 7, no. 5 (2021): e07008, https://doi.org/10.1016/j.heliyon.2021.e07008.

121. B. Şimşek Uygun and S. Malkoç, "Microplastics Biodegradation by Aspergillus Flavus and Aspergillus Versicolor," *Eurasian Journal of Biological and Chemical Sciences* 7, no. 1 (2024): 5–9, https://doi.org/10.46239/ejbcs.1374947.

122. P. R. Sutkar, S. S. Hadkar, S. A. Kamble, and V. P. Dhulap, "Biodegradation Potential of Low-Density Polyethylene (LDPE) Using *Aspergillus NIGER* and Phanerochaete Chrysosporium," *Discover Environment* 3, no. 1 (2025): 7, https://doi.org/10.1007/s44274-025-00188-9.

123. R. Usha, T. Sangeetha, and M. Palaniswamy, "Screening of Polyethylene Degrading Microorganisms From Garbage Soil," *Libyan Agriculture Research Center Journal International* 2, no. 4 (2011): 200–204.

124. M. Koutny, M. Sancelme, C. Dabin, N. Pichon, A.-M. Delort, and J. Lemaire, "Acquired Biodegradability of Polyethylenes Containing Pro-Oxidant Additives," *Polymer Degradation and Stability* 91, no. 7 (2006): 1495–1503, https://doi.org/10.1016/j.polymdegradstab.2005.10.007.

125. R. Sangeetha Devi, V. Rajesh Kannan, D. Nivas, K. Kannan, S. Chandru, and A. Robert Antony, "Biodegradation of HDPE by Aspergillus spp. From Marine Ecosystem of Gulf of Mannar, India," *Marine Pollution Bulletin* 96, no. 1–2 (2015): 32–40, https://doi.org/10.1016/j.marpolbul.2015.05.050.